Thesis for the degree of Doctor of Philosophy[1]

Inertial collisions in random flows

Kristian Gustafsson

Department of Physics
University of Gothenburg
Göteborg, Sweden 2011

[1]The thesis is available at `http://fy.chalmers.se/~f99krgu/PhdKristian.pdf`

Front cover Snapshot of $2 \cdot 10^6$ initially uniformly distributed noninteracting particles that have been dragged by an incompressible random velocity field for some time. Blue corresponds to high particle concentration and red corresponds to low particle concentration (white regions are approximately empty). Even though the velocity field is incompressible, the particles form a structure, a so called 'fractal'. One can also see lines where concentrations of particles with different velocities cross, so called 'caustics'. These are effects of the particle inertia and affect the rate at which the particles collide. The pattern is negligibly correlated to the instantaneous flow structure. Parameters: $\mathrm{Ku} = 0.1$, $\mathrm{St} = 10$, $t = 10^4\tau$.

ISBN 978-91-628-8248-8

E-publication `http://hdl.handle.net/2077/25190`

Chalmers reproservice
Göteborg 2011

Inertial collisions in random flows

Kristian Gustafsson
Department of Physics
University of Gothenburg
SE-412 96 Göteborg, Sweden

Abstract

In nature, suspensions of small particles in fluids are common. An important example are rain droplets suspended in turbulent clouds. Such clouds can start to rain very quickly and the reason for this is still not fully explained, but it is believed that the turbulent motion in the cloud plays an important role. This thesis gives an introduction to the model we use to describe inertial particles suspended in such systems and some results coming from this model.

We identify a general behavior of the particle motion which is asymptotically correct independent of how the fluid velocity is generated and on the equation of motion of the suspended particles. This asymptotic behavior can be matched to other limiting cases where the details of the system are important. This allows us to calculate an asymptotically correct distribution of particle separations and relative velocities in a form which is universally valid. The form of the distribution depends on the phase-space fractal dimension, which describes the degree upon which particles cluster in phase-space, and on d scales at which the asymptotes are matched, where d is the spatial dimension. If the fluid velocity gradients consist of white-noise, the phase-space fractal dimension and the single matching scale can be calculated analytically in one spatial dimension.

We introduce a new series expansion around deterministic particle trajectories. The expansion is done in terms of the magnitude of typical fluctuations of the fluid velocity at a fixed position. If typical fluctuations are small, we can calculate statistical quantities averaged along particle trajectories. In particular, we can calculate the degree of clustering for particles of general inertia in this limit.

This thesis consists of an introductory text and the following six appended research papers, henceforth referred to as [I], [V], [VI], [II], [III] and [IV]:

[I] K. Gustavsson, B. Mehlig, M. Wilkinson and V. Uski, *Variable-Range projection model for turbulence driven collisions*, Phys. Rev. Lett. **101**, 174503 (2008).

[II] K. Gustavsson and B. Mehlig, *Distribution of relative velocities in turbulent aerosols* arXiv:1012.1789 (2010)
Submitted to Physical Review Letters

[III] K. Gustavsson and B. Mehlig, *Relative velocities of inertial particles in random flows* (2011)
Preprint

[IV] K. Gustavsson and B. Mehlig, *Ergodic and non-ergodic clustering of inertial particles* arXiv:1101.0371 (2011)
Submitted to Physical Review Letters

[V] M. Wilkinson, B. Mehlig and K. Gustavsson, *Correlation dimension of inertial particles in random flows* Europhys. Lett. **89**, 50002 (2010)

[VI] M. Wilkinson, B. Mehlig, K. Gustavsson and E. Werner, *Clustering of exponentially separating trajectories* arXiv:1001.2788 (2010)
Submitted to European Physical Journal B

In addition a separate Licentiate thesis [1] presents the research papers [2–4].

Acknowledgments

It is my greatest pleasure to thank my supervisor Bernhard Mehlig for a never-ending support throughout my Phd time. By you reading this text means that we made it in time before summer against all odds. I look forward to our continued work together.

Next, I would like to thank all the Master students who I have had the opportunity to work with. The name list has grown over the years, thank you Björn Andersson, Andreas Skyman, Charles-Antoine Poncet, Mehdi Vahab, Habib Talavatifard, Erik Werner and Jonas Einarsson for many interesting discussions and good times. In particular I am grateful to my Chief Executive Proof Reader, Jonas Einarsson, for doing a great job spotting the biggest flaws in this thesis, even when it was in bullet-point format. I also wish to thank our international collaborators Michael Wilkinson and Vlad Bezuglyy at the Open University, Elena Meneguz at the University of Newcastle (I hope the simulations are finished soon...) and Takaaki Monnai at the Osaka City University for new insights, excellent cooperation and for great hospitality. I am also grateful for the friendly spirit of all the people at the physics department and in our group (both old and new formation) who made the time as a Phd-student joyful. Lastly, I wish to thank my friends and family for forcing me to face the third task by nagging me with questions like 'But... what is it all good for?'.

I also acknowledge the support from Göran-Gustafsson stiftelsen, from Vetenskapsrådet and from the research initiative 'Nanoparticles in an interactive environment' at University of Gothenburg.

Kristian Gustavsson
Göteborg
May 5, 2011

Contents

1

Introduction

This thesis concerns the motion of small solid particles or liquid droplets suspended in turbulent gases, so called 'turbulent aerosols'. In order to calculate the typical rate at which the suspended particles collide, one needs to understand the relative motion between pairs of such particles. This 'collision rate' determines the distribution of particle sizes in the aerosol. This quantifies how the aerosol interacts with its surroundings. An example is the interaction between atmospheric aerosols with light which is needed in climate models [6]. It can also be found that the particle-size distribution widens, particles 'rain out' from the aerosol.

One important example is a turbulent rain cloud. In so called 'Cumulus clouds' small water droplets are suspended in turbulent air currents [7, 8]. It is not understood how micrometer size droplets grow millions of times to form millimeter size rain drops within just some ten minutes, as is empirically observed [8]. Small water droplets form and grow by condensation of water vapor on preexisting aerosol particles. Due to the increasing volume to area ratio of the droplet and due to depletion of local moisture, the growth of droplet radii slows down as droplets grow larger [7, 8]. Droplets much larger than $\sim$20 µm are affected by gravity and fall through the cloud, merging with smaller particles on the way, so called 'gravitational coalescence'. If the distribution of particle sizes is wide, many collisions occur as the large droplets fall. Gravitational coalescence is believed to be the most important mechanism for the growth of rain droplets [8]. But to grow droplets to large sizes by condensation takes long time and gives a narrow droplet size distribution which makes gravitational coalescence inefficient. Rain formation due to condensation takes many hours in contrast to what is observed. It is argued that the resolution of this contradiction is that turbulence-induced collisions

between small droplets increase their growth rate and make their size distribution broad enough to make gravitation coalescence efficient. Our aim is to increase the understanding of how the water droplets collide in turbulent clouds. This problem is the main focus of this thesis, but the model we use applies to other systems of similar character. Some examples are chemical reactions in chaotic flows [9], plankton dynamics [10, 11], optimization of combustion processes and formation of planets in accretion discs around young stars [12–14]. All these systems have in common that they regard the motion and collisions between small particles with motion driven by a complicated forcing. However, as shown in this thesis it is in certain limits possible to find general mechanisms which are valid independently of the nature of the forcing.

This thesis gives an introduction to the attached papers [I–VI] which all consider the motion and collisions of inertial particles suspended in turbulent or random flows. A separate Licentiate thesis [1] gives an introduction to the papers [2–4] which mainly consider collisions between non-inertial particles that follow the streamlines of a flow, so called 'advected particles'. A detailed introduction to turbulent systems and the 'random-flow model' we use to analyze such systems is given in [1]. To make this thesis self contained, the key concepts used in this thesis are summarized in Chapter 2, **Random-flow model**.

In Chapter 3, **General principles**, we compare the random-flow model with turbulent flows. Even though dissimilarities exist some mechanisms are expected to be valid in both random flows and turbulent flows. We introduce the content of the papers [I–VI] by putting them in the contexts of such mechanisms. First, the analytical results used in [V,VI] rely on the assumption that the flow fluctuates rapidly in time, a limit which is expected to be valid also for very inertial particles suspended in turbulent flows. Second, analytical results derived in [I–III] use the fact that the relative motion between particles of large relative speed is independent of how the flow is generated. These universal results can be matched to model specific results valid for smaller relative speeds [II, III]. Finally, in the cases where the motion is system-dependent, a systematic expansion in terms of the dimensionless flow speed (the so called 'Kubo number') can be performed [IV]. By knowledge of the flow statistics at a fixed spatial position, it is possible to calculate statistical quantities along particle trajectories for small Kubo numbers.

Finally, to understand rain formation in turbulent clouds it is necessary to understand how the water droplets collide. In [1] the rate of collisions between advected particles in random flows was studied. By use of the new results in [I–VI] this analysis is extended to the case of inertial particles in Chapter 4, **Collisions**.

2

Random-flow model

For rain drops to form in turbulent rain clouds or for planets to form in interstellar accretion disks, small particles must merge in a turbulent environment. Our aim is to model the motion and collisions between small particles suspended in turbulent aerosols to increase the understanding of how the particles grow millions or billions of times to form rain drops or even planets. The model we use is simplified to the degree that it is possible to make analytical predictions but still (hopefully) incorporates the essence of the true system. In this chapter we briefly introduce a model for the motion of and for collisions between small particles suspended in turbulent flows. This model was first studied by Deutsch in one spatial dimension [15] where he discovered a phase transition, the 'path-coalescence transition', later analytically studied in [16]. For a more thorough introduction of the model, see Chapters 2–4 in [1].

2.1 Deutsch's model

We assume small spherical particles of radius a are suspended in a spatially and temporally fluctuating velocity field $\boldsymbol{u}(\boldsymbol{r}, t)$. Each particle is centered at a time dependent position $\boldsymbol{r}(t)$ with velocity $\boldsymbol{v}(t)$. The motion of the particles is assumed to be described by 'Stokes' law' (in rain-cloud turbulence this law is valid for particle sizes of 2 µm to 30 µm [17, 18])

$$\dot{\boldsymbol{r}} = \boldsymbol{v}\,, \quad \dot{\boldsymbol{v}} = \gamma\big(\boldsymbol{u}(\boldsymbol{r}(t), t) - \boldsymbol{v}\big)\,. \tag{2.1}$$

Here $\dot{\boldsymbol{r}}$ ($\dot{\boldsymbol{v}}$) denote time derivative of $\boldsymbol{r}$ ($\boldsymbol{v}$) and $\gamma \sim a^{-2}$ is the particle 'damping rate', which quantifies the particle inertia. In the limit $\gamma \to \infty$, particles are 'advected', i.e. they immediately align to changes in $\boldsymbol{u}$ and

(2.1) may be approximated by $\dot{\boldsymbol{r}} = \boldsymbol{u}(\boldsymbol{r}(t), t)$. This is the limit studied in [1]. In this thesis we extend the focus to include particles with inertia. A finite value of γ implies a delay between fluctuations of $\boldsymbol{u}$ and changes in $\boldsymbol{v}$, particles are no longer bound to follow the fluid streamlines. This has several interesting consequences which are discussed in Chapter 3.

It should be noted that the fluid velocity $\boldsymbol{u}(\boldsymbol{r}(t), t)$ in (2.1) is evaluated at the particle position, which makes (2.1) nonlinear and difficult to solve analytically for general $\boldsymbol{u}$. For a turbulent aerosol, $\boldsymbol{u}$ satisfies the fluid dynamical 'Navier-Stokes equations'. These equations are hard to solve both analytically and numerically for large turbulent systems. Instead of obeying the Navier-Stokes equations, we choose the velocity field $\boldsymbol{u}$ to be a random function that in a statistical sense mimics some (but by no means all) characteristic properties of real turbulence. We assume that $\boldsymbol{u}$ is statistically homogeneous, isotropic, time invariant and that there is no net drift, $\langle \boldsymbol{u}(\boldsymbol{r}, t) \rangle = 0$. Second order correlation functions of $\boldsymbol{u}$ can be matched to statistical properties of turbulent flows as presented next.

Turbulent motion typically has a length scale L_0 at which some macroscopic force (convection currents in turbulent rain clouds) stirs the fluid, continuously adding kinetic energy at a rate per unit mass ε. At a much smaller length scale η, energy is dissipated into heat at the same rate ε as energy is put in at the scale L_0. The energy at scale L_0 is transported to the dissipation scale η through the 'inertial range' by successive breakdowns of eddies. An eddy of size L_0 breaks down into smaller eddies which together take on the kinetic energy of the larger eddy. These smaller eddies in turn break down into even smaller eddies which take on the kinetic energy. In the end, the kinetic energy of the initial eddy is distributed among many small eddies of size η, where the kinetic energy dissipates into heat. Since new large scale eddies are continuously produced, a turbulent system consists of a hierarchy of eddies of different sizes ranging from L_0 down to η, where larger eddies sweeps smaller eddies around [19, 20].

Distances R between pairs of points such that $\eta \ll R \ll L_0$ define the inertial range. It may span several decades, e.g. a turbulent rain cloud has $\eta \sim 10^{-3}\,\mathrm{m}$ and $L_0 \sim 10^{2}\,\mathrm{m}$ [8]. As realized by Kolmogorov in 1941 [21, 22] a single parameter ε determines all dynamical quantities in the inertial range. By dimensional analysis ($[\varepsilon] = L^2/T^3$) it is possible to show that in the inertial range $\langle \Delta \boldsymbol{u}^2 \rangle \sim (\varepsilon R)^{2/3}$, where $\langle \dots \rangle$ denotes an expectation value over a statistical ensemble, $\Delta \boldsymbol{u} \equiv \boldsymbol{u}(\boldsymbol{R}, 0) - \boldsymbol{u}(\boldsymbol{0}, 0)$ and $\boldsymbol{R}$ is the separation between two points [19, 20]. Thus, for R in the inertial range we choose the random velocity field $\boldsymbol{u}$ in (2.1) to satisfy $\langle \Delta \boldsymbol{u}^2 \rangle \sim R^{2/3}$. We denote a model with an inertial range a 'multi-scale flow model'.

In the dissipation range, $R \ll \eta$, energy is dissipated into heat due to viscous forces in the fluid. In addition to ε, the fluid-dynamic viscosity ν is relevant [21, 22]. Using dimensional analysis on ε and ν (of dimension $[\nu] = L^2/T$), it is possible to find typical dimensions of the smallest eddies in turbulent flows, the 'Kolmogorov length' $\eta \propto (\nu^3/\varepsilon)^{1/4}$, the 'Kolmogorov time' $\tau \propto (\nu/\varepsilon)^{1/2}$ and the 'Kolmogorov speed' $u_0 \propto (\nu\varepsilon)^{1/4}$. Eddies of length scales much smaller than η can not form due to dissipation [19, 20]. When we are only interested in what happens at small scales, $R \ll \eta$, we approximate the turbulent flow by the Kolmogorov size eddies, a 'single-scale flow model'. For a single-scale flow we let $L_0 = \eta$ to make it consistent with the notation of multi-scale flows.

The dynamics of a fluid is smooth, meaning that for $R \ll \eta$ the velocity field $\Delta\boldsymbol{u}$ can be series expanded as, $\Delta\boldsymbol{u} \equiv \mathbb{A}\boldsymbol{R}$, where $A_{ij} \equiv \partial_j u_i$ is the 'strain rate' of the flow. Using this property, the small R statistics of $\boldsymbol{u}$ in (2.1) must be chosen such that $\langle \Delta\boldsymbol{u}^2 \rangle \propto R^2$. This is a property shared by the multi-scale and single-scale models.

The details of how the single-scale random velocity fields are constructed are given in [1, 23, 24]. To construct a single-scale flow describing Kolmogorov scale eddies, we choose in $d = 1, 2, 3$ spatial dimensions

$$u(r,t) = u_0 \nabla\psi(r,t) \tag{2.2}$$

$$\boldsymbol{u}(\boldsymbol{r},t) = u_0 \left(\partial_y \phi(\boldsymbol{r},t)\,,\ -\partial_x \phi(\boldsymbol{r},t)\right)/\sqrt{2} \tag{2.3}$$

$$\boldsymbol{u}(\boldsymbol{r},t) = u_0 \boldsymbol{\nabla} \times \boldsymbol{A}(\boldsymbol{r},t)/\sqrt{6}\,, \tag{2.4}$$

where each of $\psi, \phi, A_1, A_2, A_3$ is an independent Gaussian distributed random function with statistics chosen to be

$$C(R,T) \equiv \langle \psi(R,T)\psi(0,0)\rangle = u_0^2 \eta^2 e^{-R^2/(2\eta^2) - T/|\tau|} \tag{2.5}$$

in this thesis. Eqs. (2.2–2.4) are normalized so that $\langle \boldsymbol{u}(0,0)^2 \rangle = u_0^2$. Most turbulent flows are incompressible, i.e. their fluid density is constant. Eqs. (2.3,2.4) are constructed to make $\boldsymbol{u}$ incompressible, non-trivial one-dimensional flows are always compressible though.

2.2 Model parameters

To keep the model as simple as possible we identify the most important model parameters. They are obtained by forming independent dimensionless combinations of the dimensionful parameters. The single scale velocity field is governed by the parameters η, τ and u_0 which can be combined into the 'Kubo number' [25, 26], $\mathrm{Ku} = u_0\tau/\eta$. Turbulent flows have $\mathrm{Ku} = u_0\tau/\eta \sim 1$, but the exact value is not known. In randomly

stirred fluids, the Kubo number can be small. It might also be possible to generate velocity fields with large values of Ku from e.g. random electromagnetic fields.

The interaction between the fluid and suspended particles are governed by the damping rate, γ, which can be combined with τ into the 'Stokes number', $\mathrm{St} = 1/(\gamma\tau)$. Turbulent rain clouds typically have $\mathrm{St} \sim 10^9 a^2$ [8] which ranges from $\sim 10^{-3}$ to $\sim 10^3$ for coalescing rain droplets. However, Eq. (2.1) is not expected to be valid for this full range of Stokes numbers. As St is increased, the model (2.1) must be modified to take into account effects of gravity and additional interactions between particles and the fluid.

Collisions between particles depend upon the particle radius a and number density n_0 of suspended particles. These can be made dimensionless as $\bar{a} = 2a/\eta$ and $\bar{n}_0 = n_0\eta^d$. Here $\bar{a}$ is a dimensionless collision distance, two spherical particles of the same size collide when their separation becomes smaller than $2a$. $\bar{n}_0$ is the typical number of particles per Kolmogorov scale eddy. For Stokes' law (2.1) to be valid $\bar{a}$ must be small and for the particles not to affect the flow, the packing fraction $\bar{n}_0\bar{a}^d$ must be small [27]. Both these conditions are satisfied for microscopic water droplets suspended in rain clouds [28, 29].

2.3 Motion of particle separations

In order to calculate the rate at which particles collide it is useful to consider the relative motion of a particle pair. Two trajectories $(\boldsymbol{r},\boldsymbol{v})$ and $(\boldsymbol{r}',\boldsymbol{v}')$ have a spatial separation $\boldsymbol{R} = \boldsymbol{r}' - \boldsymbol{r}$ and a relative velocity $\boldsymbol{V} = \boldsymbol{v}' - \boldsymbol{v}$ which are determined by subtraction of (2.1) for the two particles

$$\dot{\boldsymbol{R}} = \boldsymbol{V}\,, \quad \dot{\boldsymbol{V}} = \gamma(\Delta\boldsymbol{u}(\boldsymbol{r},\boldsymbol{R},t) - \boldsymbol{V})\,. \tag{2.6}$$

Here $\Delta\boldsymbol{u}(\boldsymbol{r},\boldsymbol{R},t) = \boldsymbol{u}(\boldsymbol{r}+\boldsymbol{R},t) - \boldsymbol{u}(\boldsymbol{r},t)$. As argued in Section 2.1, $\langle\Delta\boldsymbol{u}\rangle = 0$, and $\langle\Delta\boldsymbol{u}^2\rangle$ scales as

$$\langle\Delta\boldsymbol{u}^2\rangle \sim \begin{cases} R^2 & \text{for } R \ll \eta \\ R^{2/3} & \text{for } \eta \ll R \ll L_0 \\ \text{const.} & \text{for } R \gg L_0 \end{cases}\,. \tag{2.7}$$

We remark that when time correlations are included in (2.7), an additional R-dependence enter the inertial-range scaling because larger eddies have larger time correlations [19].

At small separations, $R \ll \eta$, Eq. (2.6) simplifies to

$$\dot{\boldsymbol{R}} = \boldsymbol{V}\,, \quad \dot{\boldsymbol{V}} = \gamma(\mathbb{A}(\boldsymbol{r},t)\boldsymbol{R} - \boldsymbol{V})\,. \tag{2.8}$$

3

General principles

In Chapter 2 we introduced Deutsch's model in which we approximate the particle motion by Stokes' law (2.1) and the fully developed turbulent velocity field by a Gaussian distributed random velocity field (2.2–2.4). But are these really appropriate approximations? Several known complications concerning the particle motion in turbulent flows are overlooked in this model. One example is 'intermittency', the time signal of a turbulent velocity component subjected to a high-pass frequency filter shows a signal with occasional large bursts [19, 30]. This is an example of intermittent behavior, the signal is only active during a fraction of the time. Intermittency results in a fluid velocity distribution which is wider than the fluid velocity distribution of a non-intermittent Gaussian random flow (which is normalized such that the second order moment equal that of the turbulent flow) [19]. Another example is that the droplet motion is more complicated than Stokes' law (2.1) due to gravitational effects, buoyancy effects, 'added mass' from the surrounding fluid etc. [27]. Is it adequate to completely neglect such complications?

In this chapter we investigate what properties of real fully developed turbulent motion are expected to be described by our model and which properties lie outside the scope of the model. This is done by first stating some observed similarities and differences between the random-flow model and numerical simulations of turbulent flows, see Section 3.1. Then we identify some universal principles which apply to a great variety of systems, including random and turbulent flows, see Section 3.2. Finally, in Section 3.3 we discuss the regions in parameter space where the particle motion is system specific and how this limit can be treated analytically, provided we know the stream correlation functions of the random or turbulent flow.

3.1 Comparison to turbulent flows

In addition to the intermittency effect discussed in the previous section, there exist several differences between the characteristic behavior of turbulent and random flows. A full review of all differences and similarities lies outside of the scope of this text. One similarity is that suspended particles in both types of flows cluster on 'fractals', see cover image. This means that instead of being evenly distributed in space, particles form a structure whose shape changes with time. The fractal structure is scale invariant, upon enlargement the enlarged picture is identical to the original image in a statistical sense (for the cover image this is true for subimages of side length one tenth the full size). Depending on how well the fractal fills space, the structure can be assigned a 'fractal dimension'. One way to define the fractal dimension is the 'Lyapunov dimension', d_1 first studied by Kaplan and Yorke [31]. It is defined in terms of the 'Lyapunov exponents', λ_i, where $i = 1, \ldots, 2d$ and λ_i are ordered as $\lambda_1 \geq \lambda_2 \geq \ldots \lambda_{2d}$. These determine the exponential rates at which infinitesimal separations (λ_1), areas ($\lambda_1 + \lambda_2$), volumes ($\lambda_1 + \lambda_2 + \lambda_3$), etc. spanned between suspended particles grow or shrink at large times [32]. If e.g. areas grow but volumes shrink at large times, particles cluster on a structure which fills space better than an area of dimension two but worse than a volume of dimension three, the Lyapunov dimension takes values between two and three. For incompressible flows in three spatial dimensions, the Lyapunov dimension is defined as $d_1 = 3 - (\lambda_1 + \lambda_2 + \lambda_3)/|\lambda_3|$. Lyapunov exponents and fractal dimensions are discussed in detail in [1].

The Lyapunov exponents from numerical simulations of the random-flow model are compared to the Lyapunov exponents from numerical simulations of turbulent flows [33] in Fig. 3.1. For small St, the particles almost follow the flow and are thus sensitive to the exact flow dynamics. Depending on the correlation function of the flow, the Lyapunov exponents show different behavior as shown in Fig. 3.1. This is a 'non-ergodic effect' discussed in Section 3.3. For St much larger than the maximal value plotted in Fig. 3.1, the dynamics is universal (see Subsec. 3.2.1) and all curves in Fig. 3.1 would show the same behavior for large St. Particles in random flows with intermediate Ku show almost as large degree of clustering as particles in simulated turbulent flows. This is also true for random flows with $\tau \to 0$, a surprising fact because rapidly fluctuating flows cannot support the non-ergodic effects [26]. One significant difference between random and turbulent flows is that the second Lyapunov exponent λ_2 goes to a finite value as $\mathrm{St} \to 0$ in turbulent flows whereas λ_2 goes to zero in random flows. This is a consequence of the time irreversibility of the turbulent motion [33, 34].

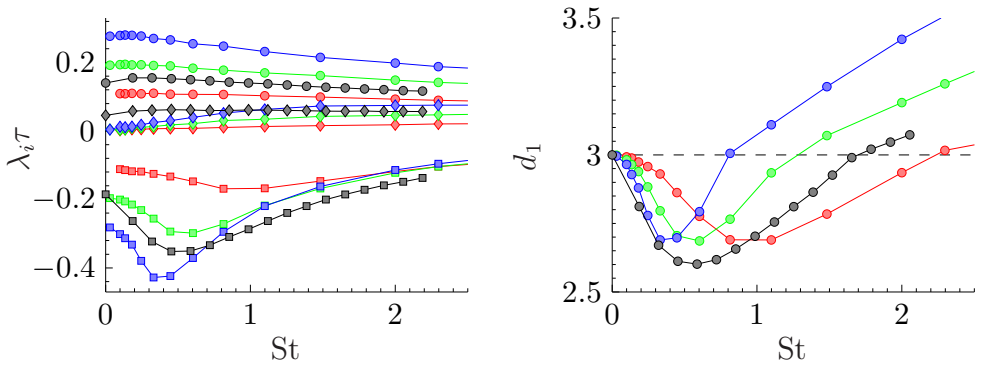

Figure 3.1: Comparison of the Lyapunov exponents for a random flow to the Lyapunov exponents for simulations of turbulent flows in three spatial dimensions [33]. Left: Lyapunov exponents λ_1 ($\circ$), λ_2 ($\Diamond$) and λ_3 ($\square$) from direct numerical simulations of turbulent flows (black), for random flows with Ku = 0.4 (red), Ku = 0.6 (green) and Ku = 0.8 (blue). Right: Lyapunov dimension d_1 with same color coding as in left panel. The correlation times of the random flow and in the turbulent simulation are expected to differ by an unknown factor, meaning St and $\lambda_i\tau$ of the turbulent simulation data should be rescaled to be comparable to the random flow data. Data for turbulent flows reproduced from [33] with kind permission from J. Bec.

3.2 Universal principles

Although the random velocity field shows some differences to turbulent flows there are general principles that are expected to apply for the motion of particles independent of the exact nature of the background flow. In this section we present several such principles.

3.2.1 The $\tau \to 0$ ergodic limit

If the velocity field $\boldsymbol{u}(\boldsymbol{r}(t), t)$ fluctuates very rapidly along the particle trajectory $\boldsymbol{r}(t)$, its fluctuations are almost indistinguishable from the fluctuations of a position independent velocity field, $\boldsymbol{u}(\boldsymbol{r}, t) \approx \boldsymbol{u}(t)$. Here 'very rapidly' means that $\boldsymbol{r}(t) \approx$ const. during the time it takes for $\boldsymbol{u}(\boldsymbol{r}(t), t)$ to decorrelate. This can be accomplished by letting τ be much smaller than all other time scales of the system, i.e. $\mathrm{St} = 1/(\gamma\tau) \gg 1$ and $\mathrm{Ku} = u_0\tau/\eta \ll 1$. For a Gaussian random flow in one spatial dimension, a more exact analysis yields the conditions $\mathrm{St} \gg 1$ and $\mathrm{Ku} \ll \sqrt{\mathrm{St}}$ [4].We call the approximation $\boldsymbol{u}(\boldsymbol{r}, t) = \boldsymbol{u}(t)$ the '$\tau \to 0$ ergodic limit' because the fluctuations of $\boldsymbol{u}$ sampled along a particle trajectory are indistinguishable from the fluctuations at a fixed position. An alternative

ergodic limit is used in [35, IV], where the velocity field has finite τ but is evaluated at a fixed position to avoid non-ergodic effects.

A suitable choice of dimensionless coordinates ($t \to \bar{t}/\gamma$, $\boldsymbol{r} \to \bar{\boldsymbol{r}}\eta$, $\boldsymbol{v} \to \bar{\boldsymbol{v}}\eta\gamma$ and $\boldsymbol{u} \to \bar{\boldsymbol{u}}\eta\gamma$) shows that if $\mathrm{Ku} \to 0$ and $\mathrm{St} \to \infty$ such that $\mathrm{Ku}^2\mathrm{St} = \text{const.}$, the dynamics is described by one single parameter, the radial diffusion coefficient for small separations $\epsilon^2 \equiv \mathcal{D}/\gamma \equiv C_d\mathrm{Ku}^2\mathrm{St}$ with $C_1 = 3$ and $C_2 = 1/2$.

The $\tau \to 0$ ergodic limit can also be employed to describe the motion of small particle separations (2.8). In this case the strain matrix in Eq. (2.8) is approximated by $\mathbb{A}(\boldsymbol{r}(t), t) = \mathbb{A}(t)$. In the $\tau \to 0$ ergodic limit various quantities defining the droplet motion in random flows have been successfully calculated. One example is the Lyapunov exponents discussed in Section 3.1, which have been calculated in all three spatial dimensions [16, 26, 36]. In one spatial dimension the maximal Lyapunov exponent changes sign from negative to positive as ϵ becomes larger than a critical value ϵ_c. This means that an initially small separation between two particles either approaches zero exponentially for large times if $\epsilon < \epsilon_\mathrm{c}$, so called 'path coalescence', or increase exponentially for large times if $\epsilon > \epsilon_\mathrm{c}$. This phase transition was first noted in numerical simulations [15] and was later calculated analytically, $\epsilon_\mathrm{c} = 1.33\ldots$ [16].

According to the Lyapunov dimension, the fractal dimension in the one-dimensional model is either zero (path coalescence) or unity (paths diverge). In [VI] we show that even though the particle separation must grow, a finite system may still exhibit clustering. The reason is that even though particles diverge at large times, they may stay together for long times until this happens, the 'finite-time Lyapunov exponent' is negative. This clustering is confirmed by an alternative measure of the fractal dimension, the so called 'correlation dimension', d_2. It is defined as the scaling of the number of particles within a sphere of radius δ around a test particle as δ tends to zero, $P(R < \delta) \equiv \int_0^\delta \mathrm{d}R\rho(R) \sim \delta^{d_2}$. For values of ϵ slightly larger than the critical value ϵ_c, the correlation dimension takes fractional values between zero and unity which quantifies the fractal clustering, see Fig. 3.2. As ϵ passes a second critical value ϵ_{c_2}, the spatial correlation dimension saturates at unity. But the 'phase-space correlation dimension' D_2 (defined in the same way as the spatial correlation dimension but with spatial separations R replaced by phase space separations $w \equiv \sqrt{|\boldsymbol{R}|^2 + |\boldsymbol{V}/\gamma|^2}$) continues to grow towards two as $\epsilon \to \infty$ [II].

In one spatial dimension, d_2 and D_2 can be calculated analytically in the $\tau \to 0$ ergodic limit [II]. In higher dimensions they can be obtained

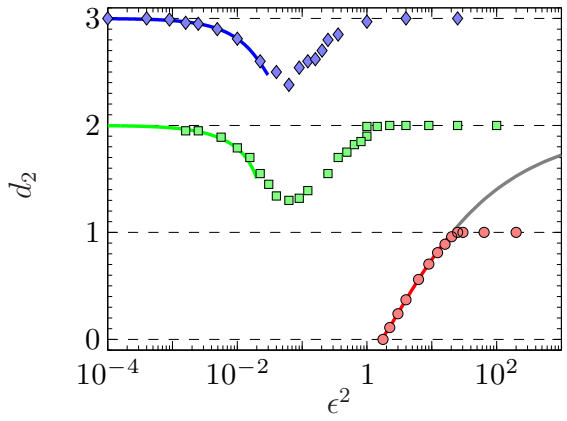

Figure 3.2: Correlation dimension in one (red,○), two (green,□) and three (blue,◇) spatial dimensions as functions of ϵ^2. Numerical simulations are data markers and theory are solid lines from [II,III], (3.1) and (3.2). The theory in one spatial dimension is extended to include the phase-space correlation dimension (gray). Simulations and theory are according to the $\tau \to 0$ ergodic limit as described in the text. The two- and three-dimensional models are incompressible, the correlation dimension approaches the spatial dimension as $\epsilon \to 0$. This is in contrast to the one-dimensional compressible model which show path coalescence ($d_2 = 0$) for all $\epsilon < \epsilon_c \approx 1.33$.

from a series expansion in ϵ

$$d_2 = 2 - 24\epsilon^2 + 528\epsilon^4 - 28800\epsilon^6 + \dots \tag{3.1}$$

for two spatial dimensions [V] and

$$d_2 = 3 - 20\epsilon^2 + 180\epsilon^4 - 9640\epsilon^6 + \dots \tag{3.2}$$

for three spatial dimensions, see Fig. 3.2.

A lowest-order correction to the correlation dimension in general dimension was found in [37]. It agrees to the lowest order correction in (3.1) but disagrees to the lowest order correction in (3.2) by a factor of two. The reason for this discrepancy is not known.

3.2.2 Caustics and variable-range projection

In the previous subsection the universality of the motion in the $\tau \to 0$ limit was discussed. In this and the next subsections we study the motion of particle pairs with relative velocities which are large compared to their separations. It turns out that this motion show universal characteristics.

Advected particles (St = 0) follow the fluid perfectly, each particle position corresponds to a single value of velocity, that of the fluid. When St > 0 by contrast, particles may detach from the fluid flow lines. The particle velocity becomes multivalued, non-colliding particles may occupy the same position in space with different velocities [38–40]. An example of this phenomenon in one spatial dimension is shown in Fig. 3.3. A density of particles is initially uniformly distributed with all particles at rest. As the particles are dragged by the velocity field, the phase-space manifold containing the particle density smoothly changes shape (Fig. 3.3 **b**). As time increases it may happen that fast particles overtake slower particles, the phase-space manifold folds over as shown in Fig. 3.3 **c** and **d**.

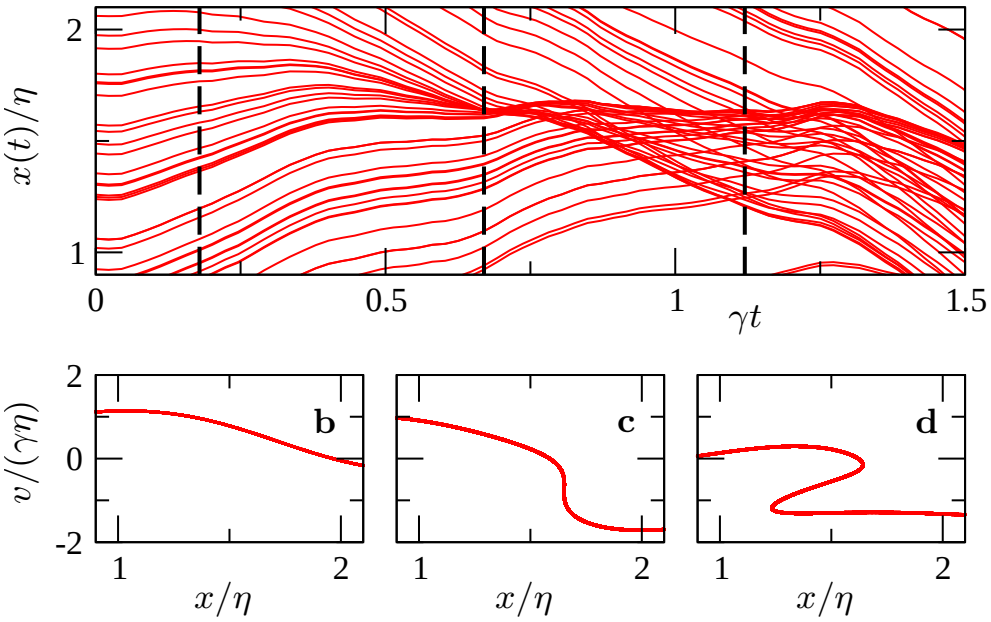

Figure 3.3: Panel **a** shows trajectories of particles in one spatial dimension following Eq. (2.1). At $\gamma t \approx 0.7$ a caustic occurs. Panels **b**–**d** show particle velocities against their positions at three different times. At the caustic, this function develops a fold.

The singular points where the phase-space manifold acquire infinite slope $\partial v/\partial x \to \pm\infty$ are referred to as 'caustics'. As shown in Fig. 3.3 **d**, caustics in one spatial dimension are always formed in pairs. Between a pair of caustics the particle velocity field is multi-valued, particles that come from far away tend to cross the caustics at large relative velocity, Fig. 3.3 **a**. If particles were allowed to collide, they would do so at high rate and with large relative velocities [38–40]. Collisions due to caustics is discussed in Section 4.3.

Consider the relative motion between pairs of particles in one spatial dimension. The aim is to find the distribution of large relative velocities, $|V| \gg \eta\gamma$, at small separations, $|X| \ll \eta$, where collisions occur, i.e. to find $\rho(|X| \ll \eta, |V| \gg \eta\gamma)$. As caustics form, particle pairs of initially large separations and large relative velocities of opposite sign are projected to (and past) small separations. Given a distribution of large $|X|$ and large $|V|$, how does this distribution change as particles are projected by caustics to small $|X|$? This question was answered in [I] using a 'variable-range projection' model [1]. In [I], the motion of particles with large values of St suspended in a multi-scale velocity field was considered. For the particles to gain large relative velocity, they typically start at large separations because $\langle \Delta u^2 \rangle \sim |X|^{2/3}$ in the inertial range (2.7). At large separations, the relative velocity V of the particles is argued to be Gaussian distributed with variance $\sim |X|^{2/3}$ [I]. If $|V|$ is assumed to be large compared to typical fluctuations of the flow, the relative motion (2.6) can be approximated by $\dot{X} = V, \dot{V} = -\gamma V$. The solution to this equation is a linear phase-space trajectory $V = V_0 + \gamma(X_0 - X)$, where X_0 and V_0 are the initial separation and relative velocity. A particle pair that starts with relative velocity $V_0 = V - \gamma X_0$ reaches $X = 0$ with relative velocity V. The distribution of initially large separations X_0 and large relative velocities V_0, $\rho(X_0, V_0)$, is a Gaussian distribution in V_0 with variance $\sim |X_0|^{2/3}$. To find the distribution of large $|V|$ at $X = 0$, X_0 is chosen as the value which gives the largest contribution to the distribution at $X = 0$. This is accomplished by maximizing $\rho(X_0, V_0) = \rho(X_0, V - \gamma X_0)$ with respect to X_0. The optimal starting point is $X_0^* = -V/(2\gamma)$, which gives the distribution of large relative velocities up to a prefactor, $\rho(X = 0, V) \sim \exp(-\mathcal{C}|V|^{4/3}\gamma^{2/3}/\varepsilon^{2/3})$, where $\mathcal{C}$ is a constant [I]. This result can be reproduced by a microscopic model [I], it is also expected to be correct for turbulent flows for large St.

The variable-range projection is a general method that can be used to match distributions at different separations with $|V|$ large enough so that the noise can be neglected. In the next section we consider a similar but more detailed matching of the distribution $\rho(X, V)$ between large $|V/(\gamma X)|$ where caustics are important and small $|V/(\gamma X)|$ where diffusion due to the velocity field u is important.

3.2.3 Matching caustics to diffusion

The rate and velocity of collisions of a particle pair is determined by the relative motion of the two particles in the pair. To understand this

[1] The name comes from the similarity to the 'variable-range hopping' model used to calculate electrical conduction in low temperature semiconductors [41].

motion one must study the distribution $\rho(\boldsymbol{R}, \boldsymbol{V})$ of spatial separations $\boldsymbol{R}$ and relative velocities $\boldsymbol{V}$ [5, II, III]. Because of the isotropicity of the flow, ρ is expected to be independent of spatial angles, i.e. it is sufficient to analyze $\rho(R, \boldsymbol{V})$. For simplicity, we consider the distribution of identical particles which are allowed to overlap, they do not collide. This distribution is relevant for collisions if St is large as we demonstrate in Chapter 4. Throughout this subsection we adopt dimensionless units $t \to t/\gamma$, $X \to \eta X$, $V \to \eta\gamma V$ and $u \to \eta\gamma u$.

For separations much larger than L_0, the distribution $\rho(R, \boldsymbol{V})$ is expected to be independent of R. A second boundary condition for the distribution is given by 'particle interchange symmetry'. As the identical particles in a pair are interchanged, $\boldsymbol{R} \to -\boldsymbol{R}$ and $\boldsymbol{V} \to -\boldsymbol{V}$, the distribution must remain unchanged, i.e. $\rho(R, \boldsymbol{V}) = \rho(R, -\boldsymbol{V})$. In particular this condition is true as $R \to 0$. This gives rise to a boundary condition needed to determine $\rho(R, \boldsymbol{V})$. In contrast, for colliding particles which are removed after collision, a vanishing distribution for separations smaller than the sum of particle radii, $\rho(R = 2a, \boldsymbol{V}) = 0$, is an appropriate second boundary condition. The distributions of colliding and non-colliding particles are in general not equivalent. We argue however that they are similar at scales $R \gg a$ if the current of particles absorbed at $R = 2a$ is small. This is the case for the distribution of advected particles [2, 3].

As shown in [II, III] the distribution of separations between non-colliding particles has generic features. This is most easily illustrated in one spatial dimension. The distribution of one-dimensional separations X and relative velocities V, $\rho(X, V)$, can be approximated by a matching between two asymptotic limits, the cases $|V| \gg |X|$ and $|V| \ll |X|$.

First, it may happen that the particle pair reaches the regime $|V| \gg |X|$. In this regime, the particle motion is deterministic and universal. The lowest order approximation is simply uniform relative motion with constant V, see Fig. 3.4 **a**. A particle separation X of opposite sign of V shrinks until zero separation is passed at finite V, that is caustics are formed. As the separation grows, $|X|$ eventually becomes comparable to $|V|$ and the system specific stochastic-and deterministic forces becomes relevant. Because V is approximately constant when $|V| \gg |X|$, we expect that for a given V, all $|X| \ll |V|$ are equally probable. Thus $\rho(X, V)$ is roughly independent of X in this limit.

Second, if $|V| \ll |X|$ the particle position X remains approximately constant while the magnitude of V fluctuates significantly compared to its typical size. Thus, in this limit we approximate the motion by $X \approx X_0 =$ const., see Fig. 3.4 **a**. The equation of motion (2.8) then becomes $\dot{V} = \gamma(\Delta\boldsymbol{u}(x, X_0, t) - V)$. In the $\tau \to 0$ ergodic limit $\boldsymbol{u}(x, X_0, t) = \boldsymbol{u}(X_0, t)$

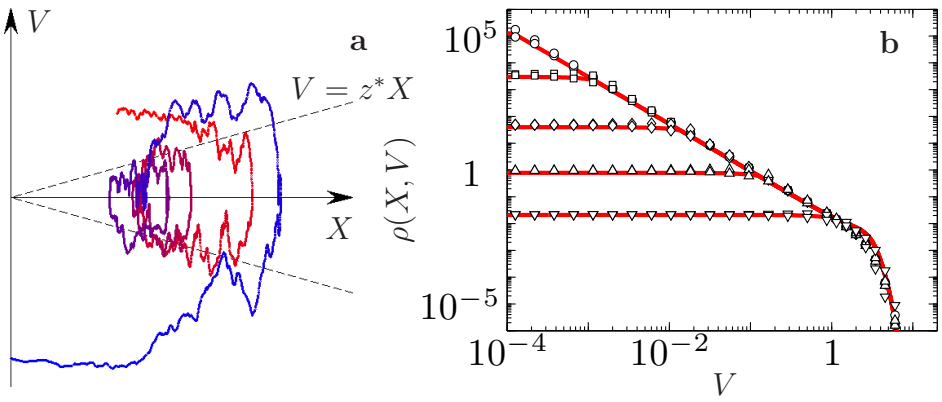

Figure 3.4: Left: A typical trajectory in one spatial dimension following Eq. (2.1). The color corresponds to running time, starting with red at $t = 0$ and ending with blue at $t = 1500\tau$. When $|V| \gg |X|$, the motion can be approximated by $V \approx$ const. and when $|V| \ll |X|$, the motion can be approximated by $X \approx$ const.. Dashed lines show the matching curves $|V| = z^*|X|$. Right: Distribution $\rho(X, V)$ plotted against V at $X = 10^{-4}$ ($\circ$), 10^{-3} ($\square$), 0.01 ($\diamond$), 0.1 ($\triangle$) and 1 ($\triangledown$). Markers are results of numerical simulations and solid lines are the asymptotic theory (3.3). The distribution is asymptotic to $|V|^{D_2-2}$ independent of X for $|V| \gg |X|$ and to $|X|^{D_2-2}$ independent of V for $|V| \ll |X|$. Parameters: Ku = 0.1, St = 100 giving $z^* = 1.26$.

which turns the equation of motion into an Ornstein-Uhlenbeck process [42]. This is a standard diffusion equation and the solution is a Gaussian in V with variance $D(X_0) = \int_{-\infty}^{\infty} \mathrm{d}t \langle \Delta u(X_0, t) \Delta u(X_0, 0) \rangle$ (c.f. Eq. (2.7)) and with a prefactor that is some function of X_0. If $|X_0|$ is small, the smoothness of the flow gives $D(|X_0| \ll \eta) \sim \epsilon^2 X_0^2$ and because $|X_0| \gg |V|$ in the limit considered, the distribution is roughly independent of V for small $|X_0|$. The Gaussian solution is specific for the $\tau \to 0$ ergodic limit where the dynamics is described by an Ornstein-Uhlenbeck process. However, the fact that the distribution is independent of V for $|X| \ll \eta$ is expected to be true for most smooth flows.

In conclusion we have the asymptotic behaviors $\rho(X, V) \sim f_I(V)$ if $|V| \gg |X|$ and $\rho(X, V) \sim f_{II}(X)$ if $|V| \ll |X|$, where f_I and f_{II} are arbitrary functions. These behaviors are clearly visible in Fig. 3.4 **b**. They are also consistent with results of numerical simulations of a one-dimensional Kraichnan model [43]. An asymptotically correct distribution for all X and V can be formed by matching the asymptotes of the distribution along some curve. As long as we are far from the system boundary, we expect a line to be a reasonable matching curve, i.e. $V = z^* X$ where

$z^* > 0$ is a parameter-dependent matching scale.

The functions f_I and f_{II} can be determined from the distribution of separations $\rho(R) \equiv \int \mathrm{d}V \rho(X,V)$ and from the distribution of phase-space separations $\rho(w) \equiv \int \mathrm{d}V \rho(w,V)$, where $w \equiv \sqrt{X^2+V^2}$. For R and w much larger than L_0, these must be constant and for R and w much smaller than η, these must scale as $\rho(R) \sim R^{d_2-1}$ and $\rho(w) \sim w^{D_2-1}$, where d_2 and D_2 are the space and phase-space correlation dimensions, both defined in Section 3.2. A natural interpolant between these limits is $D(X)$ and we find $f_I(V) \sim D(V/z^*)^{D_2/2-1}$ and $f_{II}(X) \sim D(X)^{D_2/2-1}$. In conclusion, the asymptotic distribution in the $\tau \to 0$ ergodic limit is [III]

$$\rho(X,V) = \mathcal{N} \cdot \begin{cases} D(X)^{D_2/2-1} e^{-V^2/(2D(X))} & |V| \le z^*|X| \\ D(V/z^*)^{D_2/2-1} e^{-V^2/(2D(V/z^*))} & |V| > z^*|X| \end{cases} , \quad (3.3)$$

where $\mathcal{N}$ is a normalization constant. This distribution is compared to numerical simulations of random flows in Fig. 3.4 **b**. The distribution has clear power law tails with slope $D_2 - 2$ which are cut-off for both large values of $|X|$ and for large values of $|V|$. The reason for the Gaussian cut-off of the power law tails in V is that particles are unlikely to acquire relative speeds much larger than the typical size of the fluctuations of the velocity field. The parameters D_2 and z^* can be determined analytically as functions of the diffusion coefficient ϵ^2 by a matching to an exact series solution of the distribution valid for small $|X|$ [II, III]. It should be noted that unlike the asymptotic form (3.3), the numerical distribution in Fig. 3.4 **b** is asymmetric, i.e. $\rho(X,V) \neq \rho(X,-V)$. This slight asymmetry determines the Lyapunov exponent [16].

In higher spatial dimensions it is possible to achieve similar matchings between the caustic contribution for $|\boldsymbol{V}| \gg R$ to the diffusion in $\boldsymbol{V}$ at constant R_0 for $|\boldsymbol{V}| \ll R$ [III]. In these cases D_2 has been determined for small ϵ (3.1,3.2) but we have not been able to determine the matching scales z^* analytically yet.

The asymptotic distribution of relative velocities (3.3) and the equivalent distributions in higher dimensions enable us to calculate the statistics of relative velocities needed to determine the collision rate. This is further considered in Chapter 4.

We conclude this section by a comparison of the matching that led to Eq. (3.3) to the variable-range projection used for particles with large enough St to be affected by the inertial range discussed in Subsec. 3.2.2. In the inertial range, $D(X) \sim |X|^{2/3}$ which gives rise to a velocity cut-off $e^{-\tilde{\mathcal{C}}V^{4/3}}$ instead of the Gaussian cut-off in the dissipation range. This is consistent with the result of the variable-range projection. The method presented here is equivalent to a variable-range projection with the linear

trajectories $V = V_0 + \gamma(X_0 - X)$ approximated by $V = V_0$ for large V_0. The matching of the functions $f_I(V)$ and $f_{II}(X)$ to obtain an asymptotically correct body of the distribution remains to be done for the inertial range model.

3.3 Model specific non-ergodic effects

In the $\tau \to 0$ ergodic limit of the parameter space discussed in Subsec. 3.2.1 it is possible to neglect the coordinate dependence of the velocity field $\boldsymbol{u}(\boldsymbol{r}(t), t)$ along the particle trajectory. This simplifies the analysis of the particle motion significantly. For most of the parameter space though, this is not an appropriate simplification. A standard example where the coordinate dependence in the velocity field cannot be neglected is the so-called 'Maxey centrifuge effect' [18]: Weakly inertial particles in incompressible flows tend to be centrifuged away from small scale vortices with the result that they avoid regions of high vorticity and gather in regions of high strain. Thus, particles are more likely to be found on trajectories $\boldsymbol{r}(t)$ such that the vorticity of $\boldsymbol{u}(\boldsymbol{r}(t), t)$ is low. This gives rise to non-ergodic clustering of the suspended particles, also called 'preferential concentration'. Statistical quantities (e.g. the vorticity) evaluated along particle trajectories are expected to be different from statistical quantities evaluated at a fixed position, the fluctuations are non-ergodic. Non-ergodic effects tend to be more significant the longer the particles are influenced by the same flow structure, i.e. they are expected to be most important for large values of Ku and not too large values of St. Maxey showed that the motion for small St can be approximated by advection in an effective velocity field with a compressibility proportional to $\mathrm{Tr}(\mathbb{A}^2)$. Here $\mathbb{A}$ is the strain matrix along an advected trajectory [18].

To quantify non-ergodic effects we distinguish between two different averaging methods. First, the Eulerian average is an average at a fixed position in space. We denote an Eulerian average of a quantity X by $\langle X \rangle$. This is how the statistics of the velocity field is given. Second, we denote an average of a quantity $X(\boldsymbol{r}(t))$ following a particle trajectory $\boldsymbol{r}(t)$ by $\overline{X(\boldsymbol{r}(t))}$ [2]. A statistical quantity is called ergodic if its Eulerian statistics is identical to the statistics along particle trajectories. Otherwise the quantity is called non-ergodic.

In the parts of the parameter space where non-ergodic effects are im-

[2] A third commonly used average is the Lagrangian average following a fluid element. For a trajectory with $\mathrm{St} = 0$, the particle-trajectory average equals the Lagrangian average.

portant, the exact nature of the fluid flow is important. An expansion in small values of Ku of averages along particle trajectories [IV] shows that such averages depend on gradients and higher derivatives of all orders (up to the expansion order in Ku) of the fluid potential correlation function, $C''(0,t)$, $C''''(0,t)$, ... This is in contrast to the ergodic case where the dynamics only depends on $C''(0,t)$ (or $C''''(0,t)$ for particle separations). The dependence on the nature of the fluid flow also shows in numerical simulations for large values of Ku where e.g. the Lyapunov exponents depend sensitively upon the correlation function [1], whereas they are universal functions of $C''''(0,t)$ in the ergodic limit. Thus, in the regions of parameter space where non-ergodic effects are strong, we do not expect Gaussian random flows to provide a quantitative description of for example the Lyapunov exponents or the correlation dimension, c.f. Fig. 3.1. Still, universal principles such as those discussed in Subsecs. 3.2.2 and 3.2.3 are expected to apply (although actual numerical values of e.g. D_2 and z^* depend on the nature of the flow).

3.3.1 Non-ergodic clustering

Non-ergodic statistics along particle trajectories are in general hard to calculate. In [IV] we introduce a systematic way to calculate trajectory averages by an expansion in powers of Ku. When Ku = 0, particles following Eq. (2.1) move on deterministic trajectories $\boldsymbol{r} = \boldsymbol{r}_0 + (1 - e^{-\gamma t})\boldsymbol{v}_0/\gamma$, where $\boldsymbol{r}_0$ and $\boldsymbol{v}_0$ are the initial position and velocity of the particle. As Ku is increased the deterministic trajectory is modified by addition of 'memory terms', which incorporates the effect of the velocity field $\boldsymbol{u}$ along the trajectory in terms of the initial position $\boldsymbol{r}_0$. That $\boldsymbol{u}$ is only evaluated at the fixed position $\boldsymbol{r}_0$ makes it possible to calculate statistical quantities along the trajectory assuming the statistics of $\boldsymbol{u}$ is given for a fixed position.

In [IV] we use such expansions to calculate the Lyapunov exponents for two-dimensional random flows with small values of Ku and general values of St. In the limit of small St, these can be used to explicitly calculate clustering due to the Maxey centrifuge effect. The result is consistent with that of the Maxey picture where particles are argued to be advected in an effective compressible flow with compressibility proportional to $\mathrm{Tr}(\mathbb{A}^2)$. In the limit of large St, our results are consistent with the results of the $\tau \to 0$ ergodic limit [44]. The expansion along trajectories is valid also for intermediate values of St, connecting these two limits of dissimilar character. An expansion up to sixth order in Ku turns out to be valid up to Ku ≈ 0.2. However, higher-order expansions indicate that the series is asymptotically divergent, resummation is

needed to produce results valid for Ku larger than 0.2. This is also the case for expansions in powers of epsilon in the $\tau \to 0$ ergodic limit [26]. A second limitation is that non-analytic effects coming from e.g. the multivaluedness in $\boldsymbol{v}$ due to caustics are not included in a series expansion in Ku.

In [IV] we also compare the clustering coming from non-ergodic effects such as the Maxey centrifuge mechanism to clustering resulting from the effect of many small independent accelerations in the finite τ ergodic limit. For random flows we find that the contribution to the clustering coming from a purely ergodic model is larger than the contribution from non-ergodic effects for small and intermediate Ku. This is contrary to of what is generally believed: in [45] for example it is argued that since the probability to be in straining regions in turbulent flows exhibit the same St-dependence as the correlation dimension deficit, the Maxey centrifuge mechanism alone explains clustering.

The expansion along trajectories [IV] allows to calculate many different statistical quantities in the limit of small values of Ku. It also makes it possible to treat more general equations of motion than (2.1), such as the 'Maxey-Riley equations' [27].

As a simple illustration of a problem that can be treated by the expansion in powers of Ku, consider particles in a one-dimensional random flow according to (2.2) and (2.5) with dimensionless coordinates $\bar{x} = x/\eta$, $\bar{u} = u/u_0$. The distributions of the fluid velocity $\bar{u}$ and strain rate $\bar{A} \equiv \partial_{\bar{r}}\bar{u}$ at a fixed position are independent Gaussians, $P(\bar{u}, \bar{A}) = e^{-\bar{u}^2/2-\bar{A}^2/6}/(2\pi\sqrt{3})$. One-dimensional random flows are compressible, which means that particles tend to gather in regions of the flow with high compressibility, i.e. regions where $\bar{A}$ is negative. Thus, $\overline{\bar{A}(r(t),t)}$ is expected to be negative, a non-ergodic effect because $\langle \bar{A} \rangle = 0$.

By expanding all moments $\overline{\bar{u}(r(t),t)^m \bar{A}(r(t),t)^n}$ along trajectories for small Ku like in [IV], it is possible to construct the distribution of $\bar{u}$ and $\bar{A}$ along trajectories

$$P_t(\bar{u}, \bar{A}) = \left[1 - \frac{\bar{A}\mathrm{Ku}}{1+\mathrm{St}} + \frac{(\bar{A}^2-3\bar{u}^2)\mathrm{Ku}^2(1+3\mathrm{St})}{2(1+\mathrm{St})^2(1+2\mathrm{St})} + \ldots\right] P(\bar{u}, \bar{A}), \quad (3.4)$$

where $P(\bar{u}, \bar{A})$ is the ergodic distribution stated above. This shows how non-ergodic effects deform the distributions of $\bar{u}$ and $\bar{A}$ compared to the ergodic distribution by narrowing the distribution of u and shifting the distribution of A in the negative direction. It should also be noted that along trajectories, $\bar{u}$ and $\bar{A}$ are no longer independent variables. The distribution (3.4) is compared to numerics in Fig. 3.5. As seen here the magnitude of non-ergodic effects is small for small values of Ku, but as Ku becomes larger they can be significantly larger.

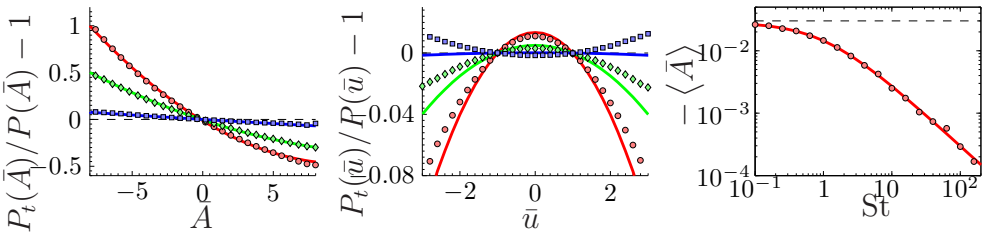

Figure 3.5: Left: Deformation of distribution of $\bar{A}$, $P_t(\bar{A}_t)/P(\bar{A}) - 1$ for Ku $= 0.1$ and St $= 0.1$ (red,$\circ$), St $= 1$ (green,$\Diamond$) and St $= 10$ (blue,$\square$). Data from numerical simulations are displayed as data markers and data from the theory (3.4) are displayed as solid lines. Black dashed line corresponds to the ergodic distribution. Middle: Same but for the distribution of $\bar{u}$. The curve does not fit as well as the distribution of $\bar{A}$. This could either be a numerical problem (very small time step is needed for the $\bar{u}$-distribution) or due to the fact that (3.4) is only the lowest order correction in Ku for $\bar{u}$. According to the numerics, the distribution of $\bar{u}$ widens when St $= 10$, a fact that is not consistent with the second order expansion (3.4). Right: Average strain of $\bar{A}$ for Ku $= 0.1$. Numerical data ($\circ$) is compared to the theory obtained from (3.4). As St approaches zero, the strain approaches the one-dimensional Lyapunov exponent $-\epsilon^2$ [1] (black dashed).

4

Collisions

To understand how aggregates of particles in turbulent aerosols form, it is necessary to study how particles collide in turbulent flows. This is the main question addressed in this thesis. It is important for a wide range of problems, e.g. the formation of rain in turbulent clouds [8, 29, 38, 40, 46] and the formation of planets in stellar accretion discs [12–14].

In our model we neglect collisions due to 'Brownian motion', in which pairs of particles collide due to thermal fluctuations of their trajectories. In turbulent rain clouds, Brownian motion is estimated to be of secondary importance to all other transport processes for particles larger than about 1 µm [17, 46], the case considered here (see however [14]).

We do not consider collisions due to gravity. As mentioned in Chapter 1, gravitational coalescence is the most important collision mechanism in turbulent rain clouds [8]. However, we want to investigate how micrometer size droplets with narrow size distribution (coming from condensation on nuclei) may grow sufficiently quickly to widen the particle-size distribution to render the gravitational coalescence efficient. Gravitational coalescence starts as some droplets become larger than ∼20 µm [7].

Results from simulations of the steady-state collision rate[1] between particles moving according to Stokes' law (2.1) in a two-dimensional incompressible random flow (2.3) is displayed in Fig. 4.1. This figure shows the rate at which one particle collides with a number of other particles. This collision rate scales linearly with the particle density n_0 (the total rate of collisions in the system is proportional to the number of particle pairs $\sim n_0^2$). Simulations of particle trajectories and counting of collisions

[1] By 'steady-state collision rate' we intend the rate of collisions for times large enough that all initial transients vanish, but with times small enough so only a small fraction of the particles collide.

are performed according to the scheme outlined in Chapter 4 and Chapter 7 in [1]. For simplicity, all particles are assumed to have the same size, i.e. they form a 'mono-disperse' system. The only interaction between particles is when they collide, i.e. when their separation becomes less than $2a$. Upon collision we consider two possibilities. Either, the particle pair is removed from the system, i.e. the particles merge and move to a larger size class (blue data in Fig. 4.1). We do not consider injection of particles from smaller size classes since the total number of collisions in the simulations is small during the total simulation time. Alternatively, upon collision the particles in the colliding pair continue to move unaffected (but overlapping) with the chance of one or multiple recollisions once their separation grows larger than $2a$ (green data in Fig. 4.1). These two cases can be seen as approximations of collisions with unit collision efficiency (blue data) or zero collision efficiency (green data). Of course, real collision processes are much more complicated, as the particles touch there are numerous different outcomes as the particles interact (collision, fragmentation, scattering into different directions etc.). The collision efficiency of rain droplets depends on their relative size and velocity in a complicated way [47].

As seen in Fig. 4.1 the collision rate is roughly constant for small values of St. As St passes a threshold the collision rate increases by orders of magnitude. This activation behavior of the collision rate as the particles grow gives a possible explanation of the rapid formation of rain in turbulent rain clouds [38, 40]. The activation behavior was argued to be caused by caustics [40]. In the following we discuss the collision rate in random and turbulent flows (Fig. 4.1) in parameter regions where the particle trajectories are well approximated by Stokes' law (2.1).

4.1 The collision rate

We define the collision rate $\mathcal{R}(t)$ as the sum of all particles entering the collision distance $2a$ of a test particle in its rest frame during a short time interval. The radial current of particles towards the test particle is

$$j_R(\boldsymbol{R}, \boldsymbol{V}, t) = -n_0 V_d(L/2)\rho(\boldsymbol{R}, \boldsymbol{V}, t)V_R(\boldsymbol{R}, t)\Theta(-V_R(\boldsymbol{R}, t))\chi(\boldsymbol{R}, \boldsymbol{V}, t)\,. \tag{4.1}$$

Here n_0 is the particle number density and $V_d(L/2)$ is the volume of a d-dimensional sphere of radius $L/2$, e.g. $V_2(r) = \pi r^2$. $\rho(\boldsymbol{R}, \boldsymbol{V}, t)$ is the probability distribution of separations $\boldsymbol{R}$ and relative velocities $\boldsymbol{V}$ to the test particle at time t. ρ is normalized to unity over the d-dimensional sphere of radius $L/2$, which means that $n_0 V_d(L/2)\rho$ is normalized to

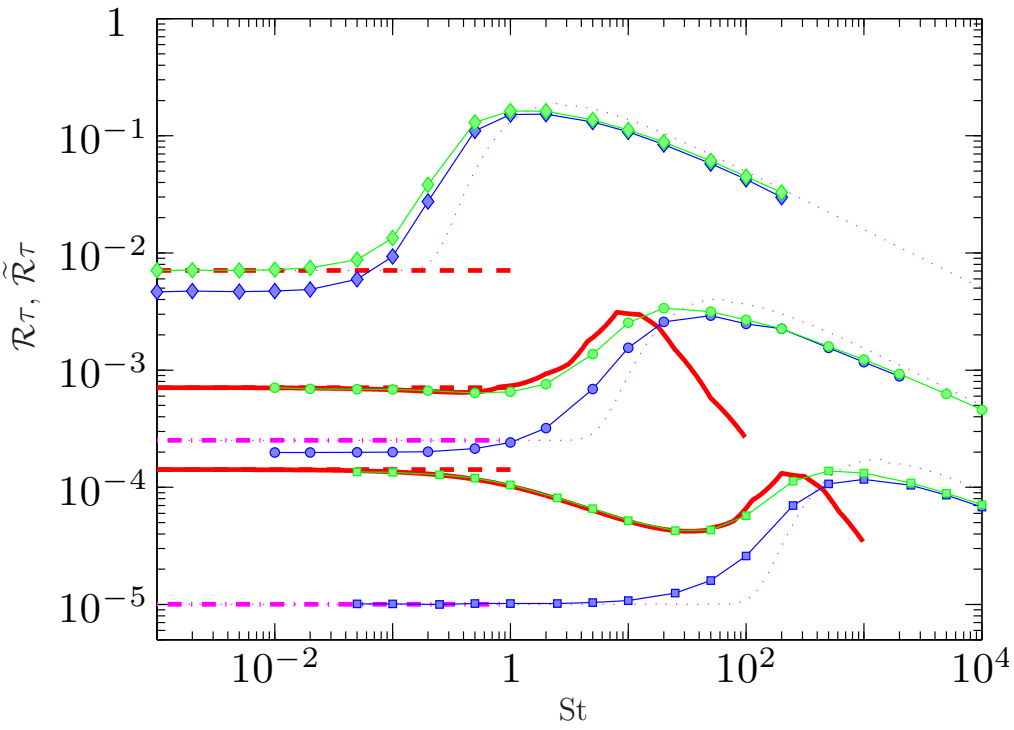

Figure 4.1: Steady state collision rates as functions of St for Ku = 0.02 (○), Ku = 0.1 (□) and Ku = 1 (◇) in two spatial dimensions. Data point markers are connected with lines. Blue data corresponds to the collision rate (4.2) and green data corresponds to the recollision rate (4.3). At St = 0 the recollision rate is given by the theory due to Saffman and Turner (4.7) (dashed red) and if also Ku is small, the collision rate approaches the advective collisions theory (4.10) (dash-dotted magenta). For small St and small Ku the recollision rate (4.9) is shown (solid red) with d_2 taken from (3.1) (for Ku = 0.1 the finite Ku result $d_2 = 2 - 12\mathrm{Ku}^2\mathrm{St}^2$ is used) and numerical data for $\epsilon > 0.1$. The ansatz (4.12) with $\mathcal{R}_s$ from (4.10) for $\mathrm{St} < \mathrm{St}^* \equiv 4S\mathrm{Ku}^2$ and $\mathcal{R}_s = 0$ for $\mathrm{St} > \mathrm{St}^*$, where St^* gives maximum of $e^{-S/\epsilon^2}\widetilde{\mathcal{R}}_g$ is plotted as (dotted magenta). Parameters are $\bar{n}_0 = 10$ and $\bar{a} = 0.02$.

the total number of particles inside the sphere. Further, $V_R \equiv \dot{R} = \boldsymbol{V} \cdot \hat{\boldsymbol{R}}$ in (4.1) is the relative radial velocity between the test particle and incoming particles and the Heaviside step function Θ selects particles moving inward. Particles which have collided with the test particle at any time during their history are absorbed and cannot contribute to the particle current. This is ensured by the indicator function $\chi(\boldsymbol{R}, \boldsymbol{V}, t)$ in (4.1). Particles at the position $(\boldsymbol{R}, \boldsymbol{V}, t)$ at time t can be identified with their trajectories $(\boldsymbol{R}(t'), \boldsymbol{V}(t'), t')$ for all $0 \leq t' \leq t$. χ indicates whether particles identified with a specific trajectory have collided with the test particle in the past. χ is unity at $t = 0$ and it is set to zero for particles that have collided with the test particle, i.e. have had a separation smaller than the collision radius $R < 2a$ at any time throughout their history.

The collision rate is given by the total flux of particles entering the collision sphere of radius $R = 2a$ is

$$\mathcal{R}(t) = \int \mathrm{d}\boldsymbol{V} \int \mathrm{d}\Omega(\boldsymbol{R})\, j_R(\boldsymbol{R}, \boldsymbol{V}, t)|_{R=2a} \,, \tag{4.2}$$

where $\mathrm{d}\Omega(\boldsymbol{R})$ is the surface element of spherical coordinates at $R = 2a$ and j_R is the ingoing radial current (4.1). In this work (with the exception of [1, 3]) we only consider steady-state collision rates, $\mathcal{R} \equiv \lim_{t\to\infty} \mathcal{R}(t)$.

The indicator function χ avoids overcounting of the collision rate, if χ is replaced by unity, all recollisions between a given particle and the test particle contribute to Eq. (4.2). But, if the collision efficiency is unity, only the first collision should be counted. It should be noted that the coordinates for which χ is zero changes with time as the particles move around. Because χ depends on the history of the particle trajectories the collision rate (4.2) is generally hard to evaluate analytically. Luckily, inertial particles tend to avoid recollisions as seen in Fig. 4.1. For large values of St (how large depends on $\bar{a}$) the curve with recollisions ($\chi = 1$) approaches the actual collision rate up to a reasonably small residual factor. Thus, when constructing a theory valid for large St it is sufficient to consider the 'recollision rate', $\widetilde{\mathcal{R}}$, defined by Eq. (4.2) with $\chi = 1$ [2]

$$\begin{aligned}\widetilde{\mathcal{R}} &= -n_0 V_d (L/2) \int \mathrm{d}V_R\, \rho(R, V_R, t) V_R(R) \Theta(-V_R(R))|_{R=2a} \\ &= -n_0 V_d (L/2) \rho(R = 2a)\, \langle V_R(R) \Theta(-V_R(R)) \rangle|_{R=2a} \,. \end{aligned} \tag{4.3}$$

In Eq. (4.3) we have assumed that the flow is isotropic and integrated out all angular dependencies. If $\rho(R)$ is uniformly distributed for $R <$

[2] Approximating $\chi = 1$ is also reasonable if one is only interested in the collision rate for short times, before recollisions have had time to occur, or if the collision efficiency is small.

$L/2$, i.e. $\rho(R) = d2^d R^{d-1}/L^d$, the recollision rate (4.3) can be further simplified

$$\widetilde{\mathcal{R}} = n_0 A_d(2a)\langle -V_R \Theta(-V_R)\rangle|_{R=2a}\,, \tag{4.4}$$

where $A_d(2a)$ is the area of a d-dimensional sphere of radius $2a$, e.g. $A_3(r) = 4\pi r^2$. The recollision rate (4.3) is commonly used to calculate the collision rate.However, the approximation (4.3) is not valid for small values of St and certainly not when also Ku is small, as seen in Fig. 4.1.

4.2 Smooth collisions

The collision rate in random flows has been calculated for advected particles in the special cases of small times (the recollision rate) [3, 29] and for small values of Ku [2, 3]. These cases of 'advective collisions' are discussed in detail in [1]. In this thesis we extend the scope to collisions between particles with arbitrary St. The finite inertia allows the particles to detach from the fluid stream lines giving rise to clustering (see Section 3.3 and caustics (see Section 3.2) as a consequence. As was argued by Maxey [18], particles with small value of St may appear as if advected in an effective compressible velocity field. It is thus expected that the theory developed for the advective collisions in a compressible velocity field should apply also to the case of small St with a few modifications. This case is considered in this section, collisions between particles where caustics are dominant is considered in Section 4.3.

4.2.1 Recollision rate at small values of St

For small values of St, caustics are rare and can be neglected. Still, finite-size particles may gain negative relative speed and collide even when St = 0 due to smooth deformations of nearby fluid elements [29, 48]. The radial projection of the relative velocity, $\Delta u_R \equiv \Delta \boldsymbol{u} \cdot \hat{\boldsymbol{R}}$, for small separations in incompressible random flows can be found from the potentials defined in Section 2.1

$$\left\langle \Delta u_R^2 \right\rangle \sim N_d^2 \frac{d-1}{3} C''''(0,0) R^2 = \frac{u_0^2 R^2}{d\eta^2}\,. \tag{4.5}$$

For advected particles in incompressible Gaussian random flows, the distribution of Δu_R is Gaussian (as opposed to compressible Gaussian random flows which have modified statistics when St = 0, c.f. Eq. (3.4)). If the distribution of V_R and R is Gaussian at $R = 2a$ it is possible to

simplify Eq. (4.4) by use of

$$\langle -V_R\Theta(-V_R)\rangle|_{R=2a} = \sqrt{\langle V_R^2\rangle/(2\pi)}|_{R=2a}\,. \tag{4.6}$$

For advected particles, $V_R = \Delta u_R$ and thus by use of (4.5) in (4.6) the recollision rate (4.4) for advected particles becomes [3, 29]

$$\widetilde{\mathcal{R}}\tau = \frac{\bar{n}_0}{\sqrt{2d\pi}} A_d(\bar{a})\bar{a}\mathrm{Ku}\,. \tag{4.7}$$

This recollision rate is equivalent to the expression found by Saffman & Turner [29]. It has for a long time been widely accepted as being correct in the advected limit of turbulent flows. However, as we showed in [2, 3], in a fluctuating flow where particle pairs are not allowed to collide multiple times, the Saffman-Turner collision rate is incorrect. This fact ($\mathcal{R} \neq \widetilde{\mathcal{R}}$ at $\mathrm{St} = 0$) is clearly visible in Fig. 4.1.

The recollision rate (4.7) can be generalized to finite values of St and small values of Ku by an expansion along trajectories, as in [IV]. We find that to lowest order in Ku, the variance of the relative radial speed is $\langle V_R^2\rangle = \langle \Delta \boldsymbol{u}_R^2\rangle/(1+\mathrm{St})$. When St is finite we have fractal clustering, $\rho(R) \sim R^{d_2-1}$ for small separations R, with correlation dimension d_2 given by (3.1) for small values of Ku and ϵ. This distribution is matched to uniform probability density $\rho(R) \sim R^{d-1}$ for large R at the matching scale R^* of the radial diffusion coefficient in (2.7) ($R^* = \sqrt{2/3}$ in $d = 1$ dimension and $R^* = \sqrt{2}$ in $d = 2$ dimensions for the velocity fields used in this thesis). Normalization gives

$$\rho(R = \bar{a}) = \frac{dd_2R^{*d-d_2}}{d_2(L/2)^d + R^{*d}(d-d_2)} \cdot \begin{cases} R^{d_2-1} & \text{if } R \leq R^* \\ R^{d-1}R^{*d_2-d} & \text{if } R > R^* \end{cases} \tag{4.8}$$

to be used in Eq. (4.3). Assuming that the distribution of V_R is close to a Gaussian, we obtain to lowest order in Ku (using (4.6) in Eq. (4.3) with $a \ll \eta \ll L$)

$$\widetilde{\mathcal{R}}\tau = \frac{\bar{n}_0 A_d(1)\bar{a}^{d_2}R^{*d-d_2}\mathrm{Ku}}{\sqrt{2d\pi(1+\mathrm{St})}}\,. \tag{4.9}$$

This expression is different from the $\mathrm{St} = 0$ expression (4.7) in two respects. First, its radial dependence scales with the correlation dimension, $\bar{a}^{d_2}$, as expected in a system with spatial clustering. This gives a larger contribution than the equivalent factor, $\bar{a}^d$ in Eq. (4.7). Second, the reduction of typical relative speeds gives the factor $(1+\mathrm{St})^{-1/2} \sim 1 - \mathrm{St}/2$.

Unless $\bar{a}$ is very small, this factor is the main modification of (4.7) for small values of Ku and the recollision rate actually decreases as a function of small values of St if Ku is small, as seen in Fig. 4.1. This shows that in this case, the Maxey picture - which suggests that particles are advected in an effective compressible velocity field (giving a second order correction in St) - is an oversimplification.

4.2.2 Collision rate for small values of St

Recollisions are in general important in regions where the smooth contribution is dominant, i.e. we cannot neglect χ in (4.2). For advected particles in flows with small Ku, the collision rate can be calculated analytically by solving a diffusion equation for the particle distribution of separations, $\rho(R)$ [2, 3]. The effect of χ is taken into account by an absorbing boundary condition at $R = 2a$, i.e $\rho(2a) = 0$ [3]. The steady-state collision rate for advected particles in a flow with small Ku becomes [2, 3]

$$\mathcal{R}_a = \bar{n}_0 A_d(1) \lambda_1 \bar{a}^{d_2} \,. \tag{4.10}$$

Here, λ_1 is the maximal Lyapunov exponent and d_2 is the spatial correlation dimension. These can be calculated explicitly in the small-Ku advective limit [49, 50], for incompressible flows we have $d_2 = d$ and $\lambda_1 = d\mathcal{D}$.

In the Maxey centrifuge picture, particles with small Stokes numbers are advected in an effective compressible velocity field $\boldsymbol{v}$. If this was the complete picture, the collision rate for small St could be obtained from Eq. (4.10) with λ_1 and d_2 being the Lyapunov exponent and correlation dimension of particles advected in a flow with compressibility given by the average $\nabla \cdot \boldsymbol{v}$, a quantity which has second order corrections in St. However, as (4.10) suggests, the average collision speed is also related to the maximal Lyapunov exponent λ_1, which gives first order corrections in St. It is thus expected that the leading order change in the collision rate (4.10) is of first order in St in contrast to the Maxey effect. To calculate the leading order correction in St is work left to be done.

4.3 Collisions due to caustics

In the previous section we studied the collision rate due to smooth deformations of the fluid. The smooth deformations caused the particles to

[3] We expect it is possible to treat a fractional collision efficiency by looking at a superposition of the solution with absorbing boundary condition, $\rho(2a) = 0$, and a 'no current' solution which has as boundary condition that ρ is integrable at the origin.

cluster which increased the rate of collisions for small particles but also decreased the typical collision speeds by a factor $(1+\mathrm{St})^{-1/2}$. This lead to a decrease of the recollision rate as particles cluster in a field with small Ku. The collision rate on the other hand increases with St in the example shown in Fig. 4.1

If the St-dependence of the collision rate was determined by clustering only, it would peak at St of order unity and drop as the clustering is decreased as $\mathrm{St} \to \infty$. Instead, the collision rate (see Fig. 4.1) is increased by orders of magnitude when St passes a threshold and then it decreases only slowly as St is further increased. In this section we explain this behavior by analyzing collisions due to caustics. Such an analysis was first attempted in [40]. Here we refine the results in [40] and compare them to the results from the distribution of separations and relative velocities in Subsec. 3.2.3.

When caustics occur, particle velocities become multivalued as illustrated in Fig. 3.3. As the pair of singularities continues to move, particles between the caustics collide with large relative velocities, independent of the particle size, Fig. 3.3 **d**. This is in contrast to smooth collisions. In this case, the relative velocity scales as $a/\sqrt{1+\mathrm{St}}$ for small a. Since collisions due to caustics occur with large relative velocities, recollisions are few if the total number of collisions are few, which allows us to approximate $\chi = 1$ and thus to use the recollision rate (4.4).

4.3.1 Caustic collision rate

Caustics form when a component R_i of particle separations passes zero with finite V_i. The frequency at which this happens has been calculated analytically in the $\tau \to 0$ ergodic limit [16, 36, 39]. For small values of ϵ the caustic formation rate $\mathcal{J}$ behaves as $\mathcal{J} \sim e^{-S/\epsilon^2}$, where S depends on the spatial dimension and, as numerical simulations show, the Kubo number. The rate of caustic formation $\mathcal{J}$ shows an activated behavior[4], it is close to zero for $\epsilon^2 \ll S$ and increases exponentially as ϵ^2 passes S. Because the collision rate due to caustics is expected to be proportional to the rate at which the caustics form, the activated behavior of $\mathcal{J}$ explains the sudden increases in the collision rate in Fig. 4.1 [40].

In the limit of large St and ϵ it is possible to calculate the recollision rate analytically. When St is large, the spatial information in Stokes' law for particle separations (2.6) is quickly lost. The equation of motion for the relative radial velocity becomes $\dot{V}_R \approx \gamma(\Delta\boldsymbol{u}(t) \cdot \hat{\boldsymbol{R}} - V_R)$

[4]The activated formation of caustics is similar to Arrhenius chemical reaction rate $e^{-T_0/T}$, which behaves similarly when the temperature T passes a critical value T_0.

independent of the particle position and separation. This is an Ornstein-Uhlenbeck process which is solved by a Gaussian in V_R with variance approximated by the large R radial diffusion matrix (Eq. (B.26) in [1]), $\langle V_R^2\rangle \sim 2u_0^2/(d\mathrm{St})$. Since V_R is Gaussian distributed we may use (4.6) in (4.4) to obtain the large-St collision rate [40]

$$\widetilde{\mathcal{R}}_g\tau = \bar{n}_0 A_d(\bar{a})\mathrm{Ku}/\sqrt{d\pi\mathrm{St}}\,. \tag{4.11}$$

This result is equivalent to that of kinetic gas theory [40]. For turbulent flows the corresponding kinetic gas theory valid for large St has been calculated by Abrahamson [46].

Multiplying the large-St asymptote $\widetilde{\mathcal{R}}_g$ with the caustic formation rate $\mathcal{J} \sim e^{-S/\epsilon^2}$ approximates the caustic contribution to the collision rate [40]. An approximate expression for the collision rate for general St then becomes [40]

$$\mathcal{R} = \mathcal{R}_s + e^{-S/\epsilon^2}\widetilde{\mathcal{R}}_g\,. \tag{4.12}$$

Here $\mathcal{R}_s$ is the smooth collision rate discussed in Section 4.2. In [40] the Saffman-Turner estimate (4.7) with fitted proportionality coefficient was used for $\mathcal{R}_s$. As seen in Section 4.2 this is in general not a good approximation. In Fig. 4.1 we show the collision rate (4.12) with $\mathcal{R}_s$ from the advective collision rate (4.10).

4.3.2 Relative velocities

In [40] it was argued that the collision rate should be on the form (4.12), but it was not deduced by an explicit calculation. Here we show that the form (4.12) follows from the asymptotic distribution of spatial separations and relative velocities discussed in Subsec. 3.2.3. In one spatial dimension it is possible to calculate z^* and D_2 in the $\tau \to 0$ ergodic limit to determine all parameters in the asymptotic distribution (3.3). This allows us to calculate the recollision rate explicitly in one spatial dimension [III]. The result is shown in Fig. 4.2. In two spatial dimensions we have so far not been able to determine the matching scales z_r^* and z_ϕ^*.

For clarity we use dimensionless variables $\boldsymbol{R} \to \eta\boldsymbol{R}$ and $\boldsymbol{V} \to \eta\gamma\boldsymbol{V}$ throughout this section. In one and two spatial dimensions the moments $m_p(R) \equiv \int_{-\infty}^{\infty} \mathrm{d}V_R |V_R|^p \rho(R, V_R)$ are on the form

$$m_p(R) \sim B_p R^{p+D_2-1} + C_p R^{d-1} \tag{4.13}$$

for $R \ll R^*$, where R^* is the matching scale defined in Subsec. 4.2.1.

We note that $m_1(X) = 2\rho(X = 2a)\,\langle V(X)\Theta(-V(X))\rangle|_{X=2a}$ if the distribution is approximately symmetric in V at $R = 2a$. Thus, the

recollision rate (4.3) can easily be calculated from $m_1(X)$ (note that $\rho(R) = 2\rho(X)$ should be used in (4.3)). In one spatial dimension we have the following coefficients for $m_1(X)$ in (4.13), where $\rho(X)$ is the distribution given in (3.3) [III]

$$\begin{aligned} B_1 &= 2\mathcal{N}\epsilon^{D_2-2}[\epsilon^2 - (\epsilon^2 + z^{*2}/D_2)e^{-z^{*2}/(2\epsilon^2)}] \\ C_1 &= 2\mathcal{N}\epsilon^{D_2-2}R^{*D_2}(\epsilon^2 + z^{*2}/D_2)e^{-z^{*2}/(2\epsilon^2)} \end{aligned} \tag{4.14}$$

with

$$\begin{aligned} \mathcal{N}^{-1} &= \sqrt{2\pi}(R^*\epsilon)^{D_2-1}L + 4z^*\epsilon^{D_2-2}\frac{R^{*D_2}}{D_2}e^{-z^{*2}/(2\epsilon^2)} \\ &\quad + \epsilon^{D_2-1}\sqrt{8\pi}\frac{R^{*D_2}}{D_2}\left[D_2 - (D_2-1)\mathrm{erf}\left(\frac{z^*}{\sqrt{2}\epsilon}\right)\right] . \end{aligned} \tag{4.15}$$

The recollision rate calculated by the moments (4.14) inserted in (4.3) is $\widetilde{\mathcal{R}}_{\mathrm{rel.}} = n_0 L m_1(X)$ and is plotted in Fig. 4.2

For large values of ϵ we find the scalings $z^* \sim \epsilon^{1/3}$ and $D_2 \sim$ const. according to [III]. Using (4.3) this gives the recollision rate for large values of ϵ and $L \gg R^*$ as $\widetilde{\mathcal{R}}_\tau \sim \bar{n}_0 2\mathrm{Ku}\sqrt{\mathrm{St}/\pi}$, identical to the kinetic gas limit (4.11).

In two spatial dimensions it is possible to construct an asymptotic distribution just as in the one-dimensional case in Subsec. 3.2.3 [III]. For this distribution the coefficients of the first moment are [III]

$$\begin{aligned} B_1 &= \frac{2\epsilon\mathcal{N}}{D_2-1}\Big[- 2\epsilon z_\phi^*(1 - e^{-z_r^{*2}/(2\epsilon^2)})e^{-z_\phi^{*2}/(6\epsilon^2)} \\ &\quad + \sqrt{6\pi}((D_2-1)\epsilon^2(1 - e^{-z_r^{*2}/(2\epsilon^2)}) - z_r^{*2}e^{-z_r^{*2}/(2\epsilon^2)})\mathrm{erf}\left(\frac{z_\phi^*}{\sqrt{6}\epsilon}\right)\Big] \\ C_1 &= \frac{2\epsilon\mathcal{N}R^{*D_2-1}}{D_2-1}\Big[\sqrt{6\pi}(D_2-1)\epsilon^2 + 2\epsilon z_\phi^*(1 - e^{-z_r^{*2}/(2\epsilon^2)})e^{-z_\phi^{*2}/(6\epsilon^2)} \\ &\quad - \sqrt{6\pi}((D_2-1)\epsilon^2(1 - e^{-z_r^{*2}/(2\epsilon^2)}) - z_r^{*2}e^{-z_r^{*2}/(2\epsilon^2)})\mathrm{erf}\left(\frac{z_\phi^*}{\sqrt{6}\epsilon}\right)\Big] \end{aligned} \tag{4.16}$$

with

$$\begin{aligned} \mathcal{N}^{-1} &= \sqrt{3}\epsilon^2\pi R^{*D_2-2}\frac{L^2}{4} - \sqrt{3}\frac{D_2-2}{D_2}\epsilon^2\pi R^{*D_2}\mathrm{erf}\left(\frac{z_\phi^*}{\sqrt{6}\epsilon}\right)\mathrm{erf}\left(\frac{z_r^*}{\sqrt{2}\epsilon}\right) \\ &\quad + \epsilon\sqrt{2\pi}\frac{R^{*D_2}}{D_2}\left[z_\phi^* e^{-z_\phi^{*2}/(6\epsilon^2)}\mathrm{erf}\left(\frac{z_r^*}{\sqrt{2}\epsilon}\right) + \sqrt{3}z_r^* e^{-z_r^{*2}/(2\epsilon^2)}\mathrm{erf}\left(\frac{z_\phi^*}{\sqrt{6}\epsilon}\right)\right] . \end{aligned} \tag{4.17}$$

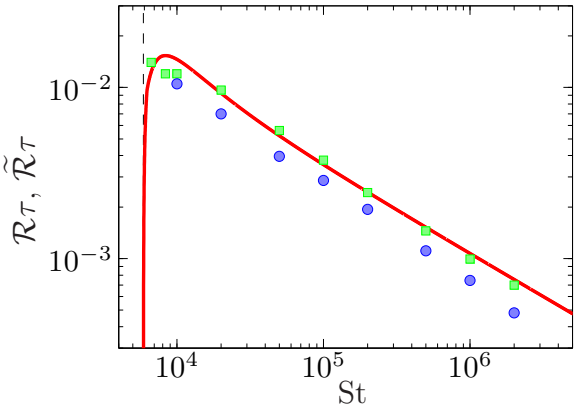

Figure 4.2: Steady state collision rate (4.2) (blue,○) and recollision rate (4.3) (green,□) in one spatial dimension as a function of $\epsilon = 3\mathrm{Ku}^2\mathrm{St}$ with $\mathrm{Ku} = 0.01$. The theory for the recollision rate according to the moments (4.13,4.14) is plotted as solid red. These data indicates that the recollision rate overcounts collisions with a non-negligible factor even for large St in one spatial dimension. The recollision rate is hard to evaluate numerically close to the path coalescence transition, $\mathrm{St_c} = \epsilon_\mathrm{c}^2/(3\mathrm{Ku}^2) \approx 5900$ (dashed black).

Just as in the one-dimensional case, the moment defined by (4.16) give the kinetic gas recollision rate (4.11) for large ϵ (assuming z_r^* and z_ϕ^* grow slower than $\epsilon^{1/2}$ as ϵ grows). To lowest order in ϵ we expect that the moment (4.16) give a collision rate which is equivalent to the large St limit of Eq. (4.9) (the $\tau \to 0$ ergodic limit). This is indeed what we find, for small values of ϵ the recollision rate (using (4.16) in (4.13)) becomes

$$\widetilde{\mathcal{R}}\tau = n_0 \bar{a}^{D_2} R^{*2-D_2} \mathrm{Ku} \sqrt{\pi/\mathrm{St}}\,. \tag{4.18}$$

which is equivalent to Eq. (4.9) because $D_2 = d_2$ for small values of ϵ.

Thus, the recollision rate calculated from the distribution of relative separations interpolates the correct limiting cases for small and large values of ϵ. To find the correct behavior in between we must determine the free parameters z_r^* and z_ϕ^*. This is work to be done, but the fact that coefficients of the type $e^{-S(z^*)/\epsilon^2}$ occurs in (4.16) gives hope that the caustic activation rate comes out as a prefactor as expected from the ansatz (4.12).

5

Conclusions

I think that the main result of the work described by this thesis is the observation and application of the universality of caustic motion. General systems with inertial particles may have the ability to form caustics, the phase-space manifold of possible particle trajectories folds over. If this happens, particles approach at separations that are much smaller than their relative speed (see Fig. 3.3), the motion is approximately uniform independent of the system in question.

This fact can be used to estimate the distribution of large relative velocities at small separations where particles collide. One example is particles inertial enough to be affected by the inertial range in turbulent flows [I]. We find that in one spatial dimension the distribution behaves as $\exp(-|V|^{4/3})$ for large relative velocities V at zero separation [I].

The universal behavior of the caustics can also be used to construct asymptotically correct distributions of particle separations and relative velocities. This is done by matching of the universal caustic motion to the motion at separations much larger than the relative velocity. In this limit the relative velocity between particles undergoes diffusion while the particle separation remains approximately constant [II,III]. The exact properties of this matching is system dependent, but some facts seem to be common by the systems we have studied. The tails of the distribution of both separations and relative velocities between particles show power law scalings with power $D_2 - 2d$, where d is the spatial dimension and D_2 is the phase-space correlation dimension, see Fig. 3.4. These power law scalings are cut off at separations comparable to the correlation length of the flow and at the scale of maximal relative velocities that can be induced by the driving force of the system.

Integration of the asymptotic distribution gives the moments (4.13)

needed to calculate the recollision rate (4.3), a quantity which is approximately equal to the collision rate for particles with large enough values of St. The found recollision rate is consistent with a sum over a smooth contribution and a caustic contribution as suggested in [40]. We can explicitly calculate the smooth contribution for small values of Ku. The caustic contribution depends on the matching scales z^*, which can be analytically calculated in one spatial dimension and matched to numerical data in two spatial dimensions. We aim to calculate z^* in higher dimensions in the near future.

A second important accomplishment is the expansion along trajectories [IV]. This allows for quantification of non-ergodic effects for particles suspended in flows with small but finite Kubo numbers. The expansion is valid for general particle inertia and it thus connects preexisting results valid for particles of low inertia to results valid for very inertial particles.

Finally, a method to calculate the spatial correlation dimension for rapidly fluctuating flows in terms of a series expansion in the noise level has been developed [V], see Fig. 3.2. The spatial correlation dimension describes the degree at which particles suspended in the flow cluster. This is an important quantity in the context of particle collisions, because collisions at small relative velocities is enhanced if particles are close in space. The surprising result that particles may cluster even though all the Lyapunov exponents in the system are positive is noted in [VI].

The main results of the work leading to the Licentiate thesis [1] is summarized in Chapter 9, **Conclusions** in [1].

In the time to come, we plan to compare the forms of the asymptotic distributions [II, III] to data from direct numerical simulations of turbulent flows and to experiments. The predictions that the distribution shows power laws in both R and V_R determined by a single parameter D_2, e.g. $\rho(R \ll |V_R|, V_R) \sim |V_R|^{D_2-d-1}$ for $D_2 < d+1$ and not too large V_R, should be straightforward to check. Further, we plan to do more calculations (both numerical and analytical) for multi-scale flows by generalizing the results in [II–IV]. For the inertial range we predict $\langle V_R^2 \rangle \sim \mathrm{St}$ [14, I], which is a result we want to compare to experiments. We also want to use the expansion in [IV] to study the Maxey-Riley equation of motion [27] which is more exact than Eq. (2.1). The expansion in [IV] allows us to incorporate effects like gravity and interactions between the particles and the fluid for small values of Ku. Finally, we want to study collisions in multi-disperse systems, where particles have different radii. In such systems, particles have different Stokes numbers which complicates the motion. It is also interesting to study the motion of non-spherical particles, but I will be busy with the points stated above so I leave this to Jonas.

Bibliography

[1] K. Gustafsson, *Advective Collisions in Random Flows*. Licentiate thesis, University of Gothenburg, Sweden, 2009. `http://fy.chalmers.se/~f99krgu/LicKristian.pdf`.

[2] B. Andersson, K. Gustavsson, B. Mehlig and M. Wilkinson, *Advective collisions*, Europhys. Lett. **80**, 69001 (2007).

[3] K. Gustavsson, B. Mehlig and M. Wilkinson, *Collisions of particles advected in random flows*, New J. Phys. **10** (2008).

[4] B. Mehlig, M. Wilkinson, V. Bezuglyy, K. Gustavsson and K. Nakamura, *Multiple regimes of diffusion*, Phys. Rev. E **80**, 011139 (2009).

[5] V. M. Alipchenkov and L. I. Zaichik, *Particle collisions in turbulent flows*, Fluid Dynamics **42** (2006).

[6] S. Solomon, D. Qin, M. Manning, Z. Chen, M. Marquis, K. B. Averyt, M. Tignor and H. M. (eds), *Contribution of Working Group I to the Fourth Assessment Report of the Intergovernmental Panel on Climate Change, 2007*. Cambridge University Press, Cambridge, UK, 2007.

[7] P. R. Jonas, *Turbulence and cloud microphysics*, Atoms. Res. **40**, 283–306 (1996).

[8] R. A. Shaw, *Particle-turbulence interactions in atmospheric clouds*, Annu. Rev. Fluid Mech. **35**, 183 (2003).

[9] A. E. Motter, Y.-C. Lai and C. Grebogi, *Reactive dynamics of inertial particles in nonhyperbolic chaotic flows*, Phys. Rev. E **68**, 056307 (2003).

[10] T. Nishikawa, Z. Toroczkai and C. Grebogi, *Advective coalescence in chaotic flows*, Phys. Rev. Lett. **87**, 038301 (2001).

[11] R. Reigada, R. M. Hillary, M. A. Bees, J. M. Sancho and F. Sagués, *Plankton blooms induced by turbulent flows*, Proc. R. Soc. Lond. B **270**, 875 (2003).

[12] A. Bracco, P.-H. Chavanis, A. Provenzale and E. Spiegel, *Particle aggregation in a turbulent Keplerian flow*, Phys. Fluids **11**, 2280 (1999).

[13] P. J. Armitage, *Lecture notes on the formation and early evolution of planetary systems*, (2007) [astro-ph/0701485].

[14] M. Wilkinson, B. Mehlig and V. Uski, *Stokes trapping and planet formation*, Astrophys. J. Suppl. **176**, 484 (2008).

[15] J. Deutsch, *Aggregation-disorder transition induced by fluctuating random forces*, J. Phys. A **18**, 1449–56 (1985).

[16] M. Wilkinson and B. Mehlig, *Path coalescense transition and its applications*, Phys. Rev. E **68**, 040101(R) (2003).

[17] H. R. Pruppacher and J. D. Klett, *Microphysics of clouds and precipitation, 2nd edition*. Kluwer Academic Publishers, Dordrecht, The Nederlands, 1997. 954p.

[18] M. R. Maxey, *The gravitational settling of aerosol particles in homogeneous turbulence and random flow fields*, J. Fluid Mech. **174**, 441–465 (1987).

[19] U. Frisch, *Turbulence*. Cambridge Univeristy Press, Cambridge, UK, 1997. 296p.

[20] G. K. Batchelor, *The theory of homogeneous turbulence*. Cambridge University Press, Cambridge, UK, 1953. 197p.

[21] A. N. Kolmogorov, *The local structure of turbulence in incompressible viscous fluid for very large Reynolds numbers*, Proceedings of the USSR Academy of Sciences (Russian) **30**, 299–303 (1941).

[22] A. N. Kolmogorov, *Dissipation of energy in locally isotropic turbulence*, Proceedings of the USSR Academy of Sciences (Russian) **32**, 16–18 (1941).

[23] A. C. Martí, J. M. Sancho, F. Sagués and A. Careta, *Langevin approach to generate synthetic turbulent flows*, Phys. Fluids **9**, 1078–84 (1997).

[24] H. Sigurgeirsson and A. M. Stuart, *A model for preferential concentration*, Phys. Fluids **14**, 4352–61 (2002).

[25] A. Brissaud and U. Frisch, *Solving linear stochastic differential equations*, JMP **15**, 524 (1974).

[26] M. Wilkinson, B. Mehlig, S. Östlund and K. P. Duncan, *Unmixing in random flows*, Phys. Fluids **19**, 113303(R) (2007).

[27] M. R. Maxey and J. J. Riley, *Equation of motion for a small rigid sphere in a nonuniform flow*, Phys. Fluids **26**, 883–889 (1983).

[28] P. S. Epstein, *On the resistance experienced by spheres in their motion through gases*, Phys. Rev. **23**, 710 (1924).

[29] P. G. Saffman and J. S. Turner, *On the collision of drops in turbulent clouds*, J. Fluid Mech. **1**, 16–30 (1956).

[30] Y. Gagne, *Contribution à l'étude expérimentale de l'intermittence de la turbulence à petite échelle*. PhD thesis, Université de Grenoble, France, 1980.

[31] J. Kaplan and J. A. Yorke, *Chaotic behavior of multidimensional difference equations*, Springer Lecture Notes in Mathematics **730**, 204–27 (1979).

[32] E. Ott, *Chaos in dynamical systems, 2nd edition*. Cambridge Univeristy Press, Cambridge, UK, 2002. 478p.

[33] J. Bec, L. Bifertale, G. Boffetta, M. Cencini, S. Musacchio and F. Toschi, *Lyapunov exponents of heavy particles in turbulence*, J. Fluid Mech. **18**, 091702 (2006).

[34] W. T. Ashurst, A. R. Kerstein, R. M. Kerr and C. H. Gibson, *Alignment of vorticity and scalar gradient with strain rate in simulated navier-stokes turbulence*, Phys. Fluids **30**, 2343–53 (1987).

[35] M. Wilkinson, *Perturbation theory for a stochastic process with Ornstein-Uhlenbeck noise*, J. Stat. Phys. **139**, 345–353 (2010).

[36] K. Duncan, B. Mehlig, S. Östlund and M. Wilkinson, *Clustering in mixing flows*, Phys. Rev. Lett. **95**, 240602 (2005).

[37] J. Bec, M. Cencini, M. Hillerbrand and K. Turitsyn, *Stochastic suspensions of heavy particles*, Physica D **237**, 2037 (2008).

[38] G. Falkovich, A. Fouxon and G. Stepanov, *Acceleration of rain initiation by cloud turbulence*, Nature **419**, 151 (2002).

[39] M. Wilkinson, B. Mehlig and V. Bezuglyy, *Caustics in turbulent aerosols*, Europhys. Lett. **71**, 186–192 (2005).

[40] M. Wilkinson, B. Mehlig and V. Bezuglyy, *Caustic activation of rain showers*, Phys. Rev. Lett. **97**, 048501 (2006).

[41] N. F. Mott, *Conduction in glasses containing transition metal ions*, J. Non-Cryst. Solids **1**, 1 (1968).

[42] H. Risken, *The Fokker-Planck Equation: Methods of solution and applications, 2nd edition*. Springer, Berlin, Germany, 1989. 472p.

[43] M. Cencini, talk *MP0806 Cencini WG3 2009.pdf* given at working group meeting of cost action mp0806, (2009).

[44] B. Mehlig and M. Wilkinson, *Coagulation by random velocity fields as a Kramers problem*, Phys. Rev. Lett. **92**, 250602 (2004).

[45] J. Bec, L. Bifertale, M. Cencini, A. Lanotte, S. Musacchio and F. Toschi, *Heavy particle concentration in turbulence at dissipative and inertial scales*, Phys. Rev. Lett. **98**, 084502 (2007).

[46] J. Abrahamson, *Collision rates of small particles in a vigorously turbulent fluid*, Chem. Eng. Sci. **30**, 1371–9 (1975).

[47] K. V. Beard and H. T. O. III, *Warm-rain initiation: An overview of microphysical mechanisms*, Springer Lecture Notes in Mathematics **32**, 608–25 (1992).

[48] M. Smoluchowski, *Versuch einer mathematischen Theorie der Koagulationskinetik kolloid Lösungen*, Zeitschrift fur Physikalische Chemie **XCII**, 129–168 (1917).

[49] E. Balkovsky, G. Falkovich and A. Fouxon, *Intermittent distribution of inertial particles in turbulent flows*, Phys. Rev. Lett. **86**, 2790–3 (2001) [`cond-mat/9912027`].

[50] Y. L. Jan, *On isotropic Brownian motions*, Z. Wahrsch. verw. Gebiete **70**, 609–20 (1985).